Comparison of Encapsulant Degradation between Glass/Backsheet and Glass/Glass Field-aged Photovoltaic Modules

by

Aesha Patel

A Thesis Presented in Partial Fulfillment
of the Requirements for the Degree
Master of Science

Approved November 2018 by the
Graduate Supervisory Committee:

Govindasamy Tamizhmani, Chair
Matthew Green
Bin Mu

ARIZONA STATE UNIVERSITY

December 2018

ABSTRACT

Ethylene vinyl acetate (EVA) is the most commonly used encapsulant in photovoltaic modules. However, EVA degrades over time and causes performance losses in PV system. Therefore, EVA degradation is a matter of concern from a durability point of view.

This work compares EVA encapsulant degradation in glass/backsheet and glass/glass field-aged PV modules. EVA was extracted from three field-aged modules (two glass/backsheet and one glass/glass modules) from three different manufacturers from various regions (cell edges, cell centers, and non-cell region) from each module based on their visual and UV Fluorescence images. Characterization techniques such as I-V measurements, Colorimetry, Different Scanning Calorimetry, Thermogravimetric Analysis, Raman spectroscopy, and Fourier Transform Infrared Spectroscopy were performed on EVA samples.

The intensity of EVA discoloration was quantified using colorimetric measurements. Module performance parameters like I_{sc} and P_{max} degradation rates were calculated from I-V measurements. Properties such as degree of crystallinity, vinyl acetate content and degree of crosslinking were calculated from DSC, TGA, and Raman measurements, respectively. Polyenes responsible for EVA browning were identified in FTIR spectra.

The results from the characterization techniques confirmed that when EVA undergoes degradation, crosslinking in EVA increases beyond 90% causing a decrease in the degree of crystallinity and an increase in vinyl acetate content of EVA. Presence of polyenes in FTIR spectra of degraded EVA confirmed the occurrence of Norrish II reaction. However, photobleaching occurred in glass/backsheet modules due to the breathable backsheet whereas no photobleaching occurred in glass/glass modules because they were

hermetically sealed. Hence, the yellowness index along with the I_{sc} and P_{max} degradation rates of EVA in glass/glass module is higher than that in glass/backsheet modules.

The results implied that more acetic acid was produced in the non-cell region due to its double layer of EVA compared to the front EVA from cell region. But, since glass/glass module is hermetically sealed, acetic acid gets entrapped inside the module further accelerating EVA degradation whereas it diffuses out through backsheet in glass/backsheet modules. Hence, it can be said that EVA might be a good encapsulant for glass/backsheet modules, but the same cannot be said for glass/glass modules.

To,

My mother-Mrs. Avani Patel, my father-Mr. Parimal Patel and my sister-Ms. Sneha Patel, for providing me with their unconditional love, support and belief in me throughout my years of study. Their words of encouragement each day have helped me in successfully completing my thesis.

ACKNOWLEDGMENTS

Foremost, I would like to express my sincere gratitude to my thesis advisor, Dr, Govindasamy Tamizhmani for giving me the golden opportunity to work in his laboratory. He has given me unending support and encouragement throughout my thesis. His patience, motivation and immense knowledge have helped me in successfully completing my thesis work. I also want to thank my thesis committee members, Dr. Matthew Green and Dr. Bin Mu for their support and guidance. I would like to thank my supervisor Dr. Archana Sinha for her unfailing support and patiently answering my queries. She consistently encouraged me to come up with my own reasonings but steered me in the right direction whenever needed. I would like to thank Sai, Ashwini, and Hamsini for helping me with the technical aspects of the laboratory equipment. My sincere thanks to Prathamesh Thorat, Shreyas Waghmare and Viswa Buddha for aiding in sample extraction. I acknowledge the use of facilities within the Eyring Materials Center at Arizona State University supported in part by NNCI-ECCS-1542160. I would like to acknowledge the Photovoltaic Reliability Laboratory (PRL)-ASU for providing me with the necessary resources for my work.

TABLE OF CONTENTS

CHAPTER Page

APPENDIX Page

List of Tables

List of Figures

Figure Page

Figure Page

Figure Page

1. INTRODUCTION

1.1. Background

Renewable energy sources have been in demand for the past few decades due to projected depletion of fossil fuels. Among the renewables, solar photovoltaics (PV) has proved to be one of the most promising renewable energy sources. Worldwide usage of PV has seen an exponential increase in the past decade [1]. A PV system comprises solar panels/modules, each consisting of solar cells (semiconductor) exhibiting the photovoltaic effect. Using the sun as a light source, a PV system works when the semiconductor absorbs the photons received from the Sun and creates electron-hole pairs to generate electricity. A PV module is nothing but a stack of layers i.e. superstrate (glass), solar cell assembly sandwiched between two layers of the encapsulant and the substrate (backsheet/glass), each contributing towards the efficiency, reliability, and durability of the module. A backsheet is a polymer or a combination of polymers which provides support to the PV module and protects the module from damage due to extreme weathering conditions such as a hailstorm, snow load, etc. However, these layers undergo degradation due to their prolonged field exposure over 25-30 years. Degradation modes like encapsulant browning, delamination, cell cracking, backsheet cracking and yellowing, hotspots, etc. are some of the commonly observed failures occurring due to subjecting the modules to high UV exposure and elevated temperatures. These failures caused a reduction in the efficiency of the PV modules. Hence, current research is more focused on the reliability of these modules. Figure 1 shows the schematic diagram of the cross-section of a PV module and their individual failure modes.

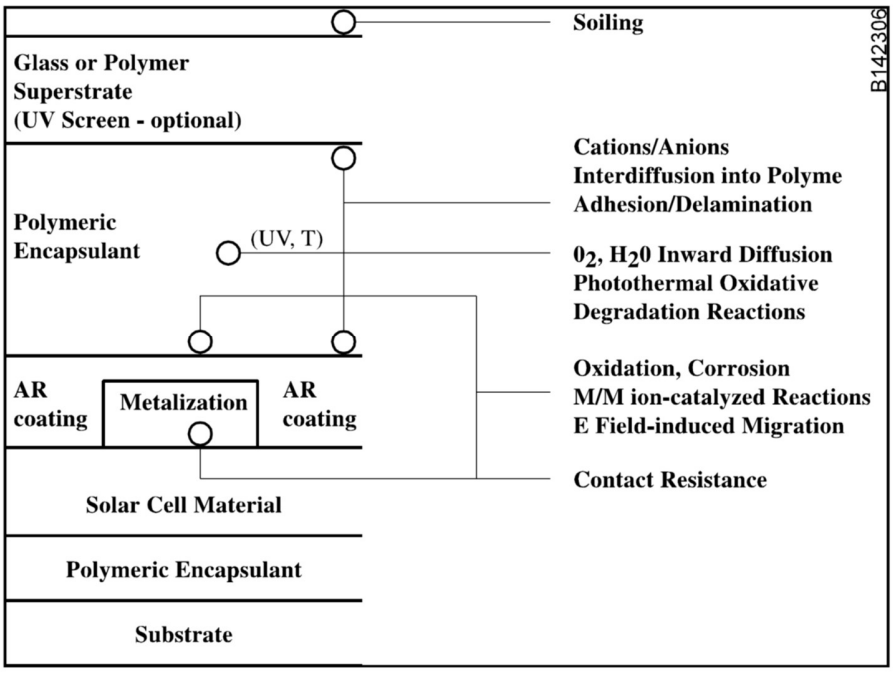

Figure 1: Schematic diagram of the cross-section of a PV module and the failure modes at each layer [2]

One of the most critical components in a PV module is the encapsulant. The purpose of an encapsulant in a PV module is to provide structural support, adhesion between different interfaces, thermal conduction, electrical isolation, optical coupling. The encapsulant is stable at high UV exposure and elevated temperatures and thereby helps the PV module to withstand such conditions. But the encapsulant being a polymeric material, it tends to degrade over time. Hence, degradation of the encapsulant is a matter of concern because it has a major contribution towards the performance loss of the module. Therefore, it is important to study the degradation of the encapsulant to predict the reliability of the module.

1.2 Problem Statement

Glass/backsheet PV modules with stabilized ethylene vinyl acetate (EVA with additives to increase its stability) as the encapsulant have been the conventional and the most dominating technology in the PV market for decades. As new technologies have surfaced, glass/glass modules seem to be favored more than glass/backsheet modules to avoid moisture/oxygen ingression, thereby preventing corrosion. Figure 2 and Figure 3 show the schematic diagram of the cross-section of stacked layers for glass/backsheet and glass/glass modules, respectively, investigated in this study.

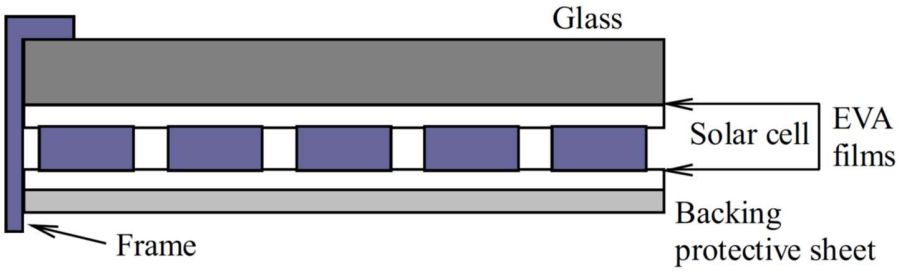

Figure 2: Schematic diagram of the cross-section of a glass/backsheet PV module [3]

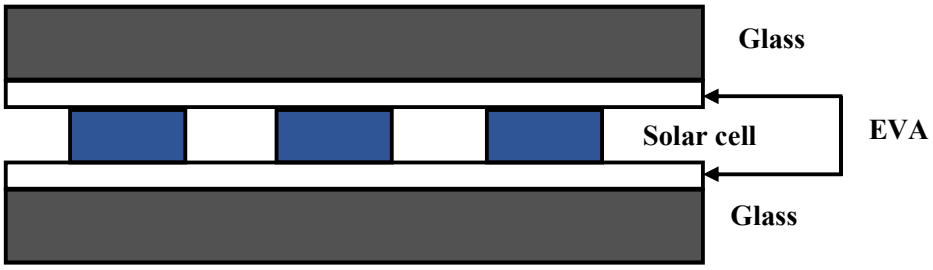

Figure 3: Schematic diagram of the cross-section of a glass/glass PV module

Since EVA is the most commonly used encapsulant in glass/backsheet modules, many manufacturers chose to use EVA as the encapsulant for glass/glass modules too. EVA being a polymer, will tend to degrade over the period due to longer exposures to elevated

temperatures and UV radiation. EVA undergoes photothermal degradation resulting in encapsulant browning and photobleaching in the presence of oxygen resulting in discoloration. Browning being one of the major failure modes in the PV module reduces the transparency of the encapsulant and eventually reducing light transmission through it. This causes performance losses. But there is a possibility that there could be a difference in the encapsulant degradation pathway and its impact on the performance on the modules due to the difference in their stacking construction. Therefore, it is important to study the comparison of EVA encapsulant degradation for glass/backsheet and glass/glass PV modules.

1.3 Objective

The main objective of my thesis is to compare the degradation of EVA encapsulant in glass/backsheet and glass/glass PV modules that have undergone difference periods of the field-exposure. Two major failure modes of the encapsulant are delamination and discoloration. The motivation of this work is to compare the effects of discoloration on the physical and chemical properties of the encapsulant and thereby on the performance parameters of the modules. Using various characterization techniques, it is possible to monitor the changes in the properties of the EVA encapsulant that is extracted from the field-aged and fresh glass/backsheet and glass/glass modules.

The objectives of this study are as follows:

- To extract EVA from a few selected regions in the field-aged modules and perform various non-destructive as well as destructive characterization techniques to study the structural and chemical changes in the EVA encapsulant with browning.
- EVA discoloration caused by longer exposures to UV radiation and elevated temperature affects the physical, chemical, and optical properties relatively. Hence, the goal is to study the changes in structural properties such as crystallinity, vinyl acetate content, and crosslinking and chemical structure such as the presence of products causing browning in EVA by performing various destructive as well as non-destructive characterization techniques.
- To monitor the deviation of performance parameters such as short circuit current (I_{sc}) and maximum power (P_{max}) from the initial to post field-aged readings because of encapsulant browning
- To correlate the structural and optical properties of glass/backsheet and glass/glass modules to study encapsulant degradation and compare them.

2. LITERATURE REVIEW

2.1 PV encapsulant

The encapsulant, being the critical component in a PV system is a major focus for research. With modules of different constructions emerging, it becomes crucial to develop new encapsulants that help in increasing the expected lifetime of the module. PV encapsulant is a polymeric material which has the following functions [4]:

- Provide adhesion between glass/solar cell and solar cell/substrate interfaces.
- Provide protection to the solar cells from environmental stresses like rain, snow, hail, etc., humidity and UV radiation.
- Structural support to the PV module design
- Maintain optical coupling between the glass and solar cell and achieve the transmittance of at least 90%.
- Provide physical and electrical isolation of the solar cells and components.

EVA is a commonly used encapsulant in PV modules. It is a semi-crystalline copolymer consisting of polyethylene (crystalline) and vinyl acetate (amorphous). Figure 4 gives the chemical structure of EVA.

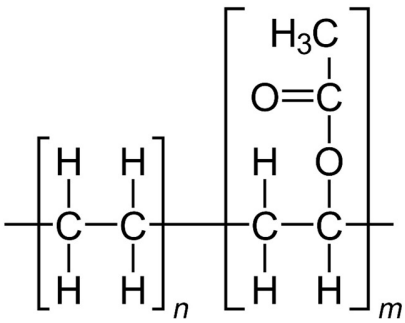

Figure 4: Chemical structure of ethylene vinyl acetate (EVA) [5]

For PV applications, EVA consists of various additives like UV absorber, UV stabilizer, anti-oxidant, and a curing agent to inhibit degradation reactions. EVA is highly favorable as an encapsulant in PV modules because of its properties. The physical properties of EVA are: high electrical resistivity, high adhesion strength, and high optical transmission. The chemical properties of EVA are: resistant to UV radiation, low water absorption ratio, non-toxic, and high thermal stability. After decades of research, PV market has come up with several encapsulants other than EVA such as polydimethylsiloxane (PDMS), poly (vinyl butyral) (PVB), thermoplastic polyolefins (TPO), ionomer, etc. However, since EVA is affordable and exhibits high durability, it has become the dominant encapsulant in the PV market.

2.2 Degradation of EVA encapsulant

Even though the commercial EVA encapsulant with additives is highly stable under UV exposure and high outdoor operating temperature, it tends to degrade over time. The two main failure modes of EVA encapsulant are delamination and discoloration. Delamination is caused due to the breaking of interfacial bonds [6] and discoloration is caused due to the depletion of additives in the encapsulant or occurrence of Norrish reactions because of elevated temperatures and high UV exposure [7], [8]. The two determining reactions of discoloration are photothermal degradation and photobleaching which take place at an unknown rate. Despite the attempts made to investigate the degradation mechanism(s) of

the EVA encapsulant caused due to UV radiation, heat and moisture/oxygen ingression, it is still not fully explained and understood in the literature.

There are two possible degradation mechanisms for EVA degradation. One of them is because of additives in EVA that cause EVA degradation. EVA is unstable under UV exposure. Hence, there are some additives added which stabilize the EVA. The common additives in EVA are Cyasorb UV 531 (UV absorber), Lupersol 101 (curing agent), Naugard P (anti-oxidant/hydroperoxide decomposer) and Tinuvin 770 (UV stabilizer) [8]. Cyasorb decomposes into unknown aromatic compounds due to photodegradation which causes an increase in crosslinking in EVA. According to the literature, Cyasorb's decomposition products absorb UV wavelength less than 300nm, hence they cannot be termed as color giving chromophores. However, researchers claim that benzoic acid is its major product but no evidence has been found from FTIR-ATR analysis so far [7]. Naugard P is not effective in reducing Cyasorb's photo-decomposition because its main function is to decompose peroxides and hydroperoxides. Tinuvin 770 is a UV stabilizer and its function is to scavenge free radicals and increase the energy barrier for the formation of acetic acid [8]. However, how Tinuvin and Naugard decompose is not known in the literature [7]. But in absence of free radical scavenger (Tinuvin), crosslinking is accelerated as it is a process initiated by a mechanism involving photogenerated free radicals [8]. However, according to the literature, Lupersol (curing agent) promotes the generation of chromophores (part of a molecule responsible for its color).

Another degradation mechanism that has stuck out is that of polyene formation causing EVA degradation. It states that the process of EVA degradation begins with the chain

scission and increase in crosslinking in EVA encapsulant due to UV irradiation [8]. Both chain scission and crosslinking occur in the vinyl acetate groups because photostability of polyethylene is higher than vinyl acetate. The stabilizers added in the EVA encapsulant are vaporized due to UV and heat which causes an increase in crosslinking and formation of volatile acetic acid and polyenes by Norrish II reaction, as given in Figure 5 [8], [9]. Crosslinking in discolored regions of EVA is increased to greater than 90% [8]. According to the literature [4], [10], the unsaturation like hydroperoxides, double bonds, and carbonyl groups called chromophores are the causes of photodegradation. Polyenes contain chromophores -[C=C]-_n which cause EVA browning. Hence longer the chain of polyenes, higher will be the browning in that region. Sometimes, chromophores cannot be detected by FTIR-ATR because of the low absorptivity of conjugated -[C=C]-_n bonds in 1500-1600 cm^{-1} region. However, longer polyenic chromophores can be detected in ATR mode [7]. Higher browning/discoloration leads to higher loss of transmission in that region, thereby affecting the efficiency of the module. Acetic acid produced by Norrish II reaction acts as a self-catalyst and accelerates the EVA degradation. Other reactions that take place are Norrish I and III reactions which give products like aldehyde, ketone, CO_2, CO, and CH_4. Crosslinking interferes with the orderly chain packing of the molecules in the EVA polymer. Hence, it reduces the crystallinity of the polymer and increases its vinyl acetate content (VAc). Increase in VAc increases the rate of deacetylation reaction, thereby increasing the production of acetic acid and polyenes. However, determining the right degradation mechanism is out of the scope of this work.

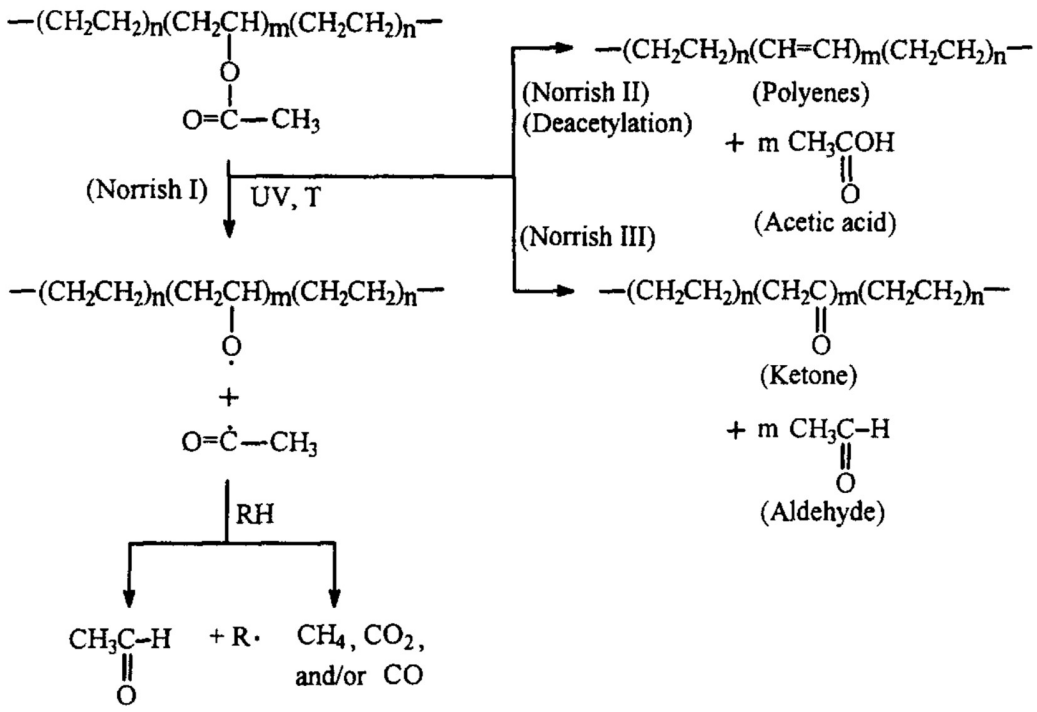

Figure 5: Norrish reactions of EVA [10]

Photobleaching occurs in the presence of moisture/oxygen which produces keto-chromophores that shorten the length of polyenes and eliminates discoloration [8]. Shortening of polyenes turns the dark brown color of EVA encapsulant into light yellow/white. Diffusion of air into the EVA is a basic requirement for the occurrence of photobleaching and it can occur at any temperature in presence of oxygen [8]. Polyene oxidation mechanism is given in Figure 6.

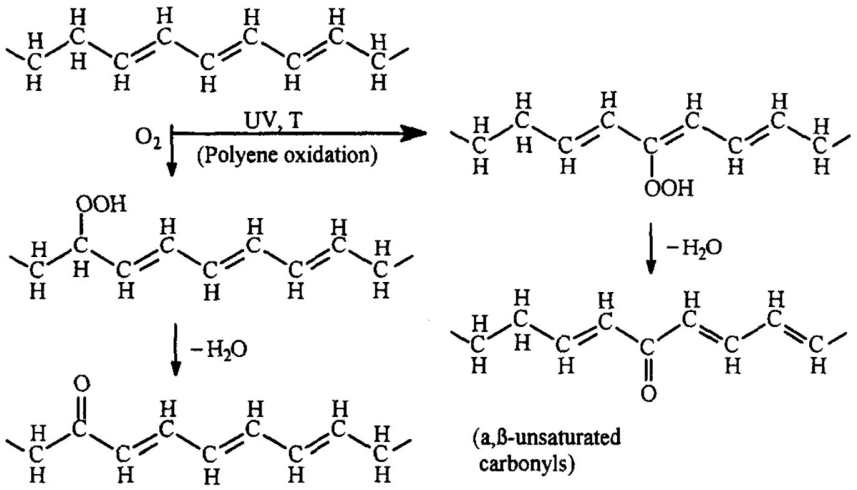

Figure 6: Photobleaching reaction mechanism of EVA browning [10]

2.3 Effects of EVA degradation

The encapsulant degradation directly affects the performance of the module and thereby its reliability. It reduces the power output and results in performances losses causing a reduction in the service life of the modules.

Delamination of encapsulant occurs if the encapsulant faces adhesion failure and causes moisture/oxygen ingression into the modules causing the formation of air bubbles. These air bubbles when entrapped between the laminate cause humidity accumulation leading to short circuits and loss of the power output [11]. They also cause corrosion of the cell metallization [12]. Moisture/oxygen ingression accelerates the corrosion of the metallic circuits of a solar cell. Discoloration of the encapsulant produces acetic acid which due to its low pH, accelerates the process of corrosion of metallic interconnects in a solar cell resulting into formation of intermetallic compounds, solder bond degradation causing an

increase in series resistance and reduction of efficiency of the module [10]. Discoloration of the EVA encapsulant causes loss of transmittance of the polymeric material. This causes lower absorption of the photons from sunlight which leads to loss of performance [4]. To avoid these drastic effects of EVA degradation on the efficiency of the modules, researchers are looking for different possible additives to use while processing to improve the properties of the EVA encapsulant.

2.4 PV encapsulant characterization

Polymer material characterization techniques are used to study the EVA encapsulant degradation. Many prefer to perform pre-characterization and post-characterization of the modules before and after exposing them to the environment, respectively. Figure 7 shows the overall picture of the characterization techniques generally used to study polymer degradation.

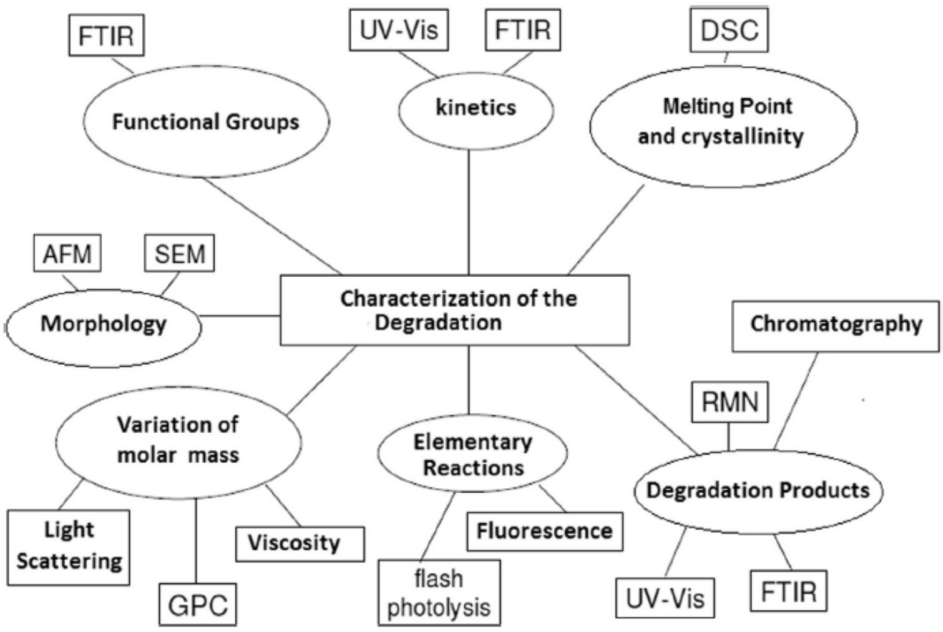

Figure 7: Characterization techniques to study polymer degradation [4]

Literature gives a wide range of methods to study the changes in physical and chemical properties of the encapsulant caused due to the degradation.

Differential Scanning Calorimetry (DSC) and Thermogravimetric Analysis (TGA) are predominant methods for thermal analysis of the encapsulant. They are generally used to study the phase behavior as well as the thermal stability of the encapsulant, respectively. Another method called Dynamic Mechanical Analysis (DMA) is used to study the viscoelastic behavior of the encapsulant. Agroui et al. (2013) used DSC to study the phase transitions of the EVA encapsulant after the completion of module encapsulation process [13]. Polansky et al. (2013) used thermal methods like DSC, TGA, and DMA to study the thermal stability of the EVA encapsulant along with the kinetic parameters of crosslinking achieved during lamination process [3].

Raman spectroscopy and Fourier transform infrared spectroscopy (FTIR) are predominant methods for monitoring changes in chemical structure and molecular vibrations of the encapsulant. FTIR characterizes the EVA encapsulant by detecting the chemical functional groups present in the degradation products. Koehl et al. (2011) used Raman spectroscopy to analyze the degraded EVA and study the effect of degradation on fluorescence background in Raman spectroscopy [14]. Peike et al. (2014) used Raman spectroscopy to study the degree of crosslinking in EVA encapsulant and compared the results with that obtained from Soxhlet extraction method which is the commonly used method for measuring gel content to analyze the degree of crosslinking [15]. Since FTIR and Raman spectroscopies are considered as complementary methods for chemical analysis, Planes et al. (2014) used these complementary methods along with DSC and TGA to study the thermal and chemical changes in the encapsulant after exposing it to an accelerated aging at 80ºC/85% RH for 2000 hours [16].

Other than the spectroscopic and thermal methods, there are many other methods which are used to determine the efficiency of the module and failure modes in the module. I-V measurements are generally taken as a part of pre-characterization and post-characterization to monitor the changes in the performance parameters of the module before and after field exposure or accelerated tests [17]. UV Fluorescence imaging gives a clear picture of the degradation modes like encapsulant browning and delamination [18]. It shows if the encapsulant has a uniform or non-uniform discoloration pattern throughout the module. Colorimetry is another method which can quantify the encapsulant discoloration [18]. These and various other characterization techniques help in studying

the reason for the variations caused in the physical, chemical and optical properties of the encapsulant.

3. METHODOLOGY

3.1 Test samples

To study the degradation mechanism of EVA encapsulant, samples were extracted from three field-aged modules of different manufacturers with different exposure periods. The details of the selected three modules are as follows:

i. Module Type I (glass/backsheet): exposed to Arizona's climate for 18 years
ii. Module Type II (glass/backsheet): exposed to Arizona's climate for 21 years
iii. Module Type III (glass/glass): exposed to Arizona's climate for 10 years.

Table 1 provides a list of EVA samples that were tested. For comparison, unexposed/fresh EVA was also tested.

Table 1: List of unexposed and exposed EVA samples to be tested

Nature of the EVA samples	**EVA sample type**	**Sample source**
Unexposed	Uncured	fresh EVA roll
	Cured	From a freshly laminated mini-module
Exposed	Cell center (front EVA)	From field-retrieved modules type I (glass/backsheet; see Figure 2 for construction details), II (glass/backsheet; see Figure 2 for
	Cell edge (front EVA)	

	Non-cell area (double layer – front and back EVA)	construction details) and III (glass/glass; see Figure 3 for construction details)

The cells to be cut from the modules were decided based on their visual and UV fluorescence images that are discussed in section 3.3.1 and section 3.3.2, respectively.

7,6, and 4 cells were cut from module type I, II, and III, respectively along with EVA from their non-cell regions.

3.2 Sample preparation

The selected cells from all three modules (type I, II and III) were cut using a diamond wheel Dremel tool attachment/snipping tool shown in Figure 8.

(a) **(b)**

Figure 8: (a) diamond wheel Dremel tool (b) snipping tool used to cut the cells from the modules

EVA was extracted from the cells by removing the other stacked layers i.e. front glass pieces, the backsheet, back EVA and the cell. After getting the front EVA separated from the cell using a scalpel, it was cleaned using the Dremel tool with a cleaning brush attachment to remove the remaining shrapnel of glass and cell as shown in Figure 9. The edge and center EVA samples were cut from the encapsulant and were wrapped in an aluminum foil and placed in an air-tight plastic bag. Plastic bag and aluminum foil were used to prevent the encapsulant from environmental exposure/hazards and the anti-static material in plastic bags called erucamide, respectively, that could affect its characterization.

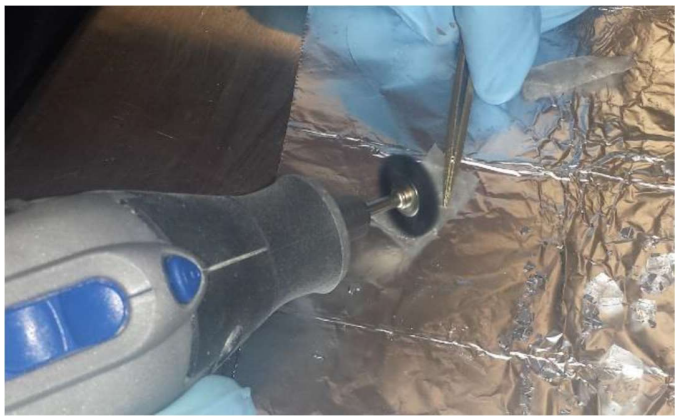

Figure 9: Plastic brush cleaning tool for cleaning the extracted EVA

3.3 Methods for EVA Characterization

To study the encapsulant degradation, EVA was characterized by a few non-destructive as well as a few destructive techniques. Some methods like colorimetry, UV fluorescence imaging, Raman spectroscopy which do not require breaking the module to extract the encapsulant are termed as non-destructive techniques whereas methods like Differential Scanning Calorimetry, Thermogravimetric Analysis, and Fourier Transform Infrared Spectroscopy which require extraction of the encapsulant by breaking the module are termed as destructive techniques. Since the purpose is to study the physical and chemical changes in the encapsulant due to field-aged degradation, characterization techniques were chosen accordingly.

3.3.1 Visual Inspection

According to the IEC standard 61215, visual inspection (VI) of a PV module is carried out to detect and locate the visual defects that could have affected the performance parameters of the module. The modules were examined visually under the condition of not less than 1000 lux illumination as per IEC 61215 standard, for the presence of discoloration and other physical deterioration in the EVA. This can be classified as one of the non-destructive methods.

3.3.2 Ultra-violet Fluorescence Imaging

Ultra-violet fluorescence (UVF) imaging is a non-destructive method used to detect encapsulant browning and delamination. The early stage of browning which cannot be

identified during the visual inspection can be detected using UVF imaging. In general, UV fluorescence occurs when the UV radiation excites the chromophores present in the material and causes them to release the visible light. In aged EVA, fluorescence is caused by the chromophores formed in the encapsulant because of its degradation. Figure 10 shows the setup for the UV fluorescence imaging. The setup includes a UV illumination system comprising of two arrays of 15 UV lamps each inclined at an angle of 45° w.r.t. the module surface so that it eliminates the glare in the images caused due to the UV light reflection. Hence, to investigate the modules for browning, the modules were illuminated by the UV light and images were taken using a digital visible camera to identify the areas which were browned.

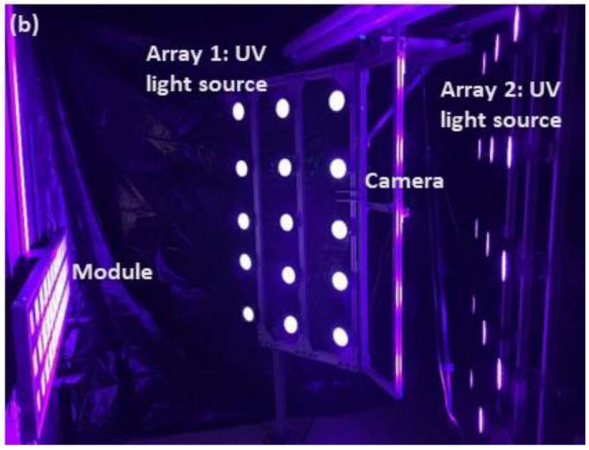

Figure 10: Experimental setup for UV fluorescence imaging

3.3.3 Current-Voltage measurement

The current-voltage (I-V) data were collected indoors using a Class A solar simulator equipped with a Xenon – arc lamp with an appropriate filter. This equipment is capable of

measuring cell-level I-V data. Before taking the I-V measurements, the room was maintained at a temperature of 25ºC. The lamp was switched on and left undisturbed for almost 20 minutes to stabilize the light source. The irradiance monitor was calibrated using a PVM 798 reference cell. The setup of a solar simulator is shown in Figure 11.

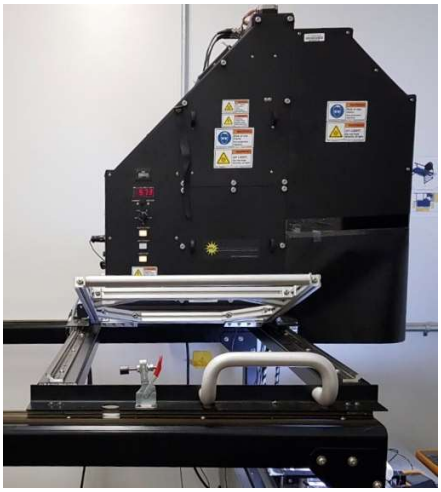

Figure 11: Experimental setup of a solar simulator for I-V measurements

To measure the cell-level I-V data, a thermocouple was attached on the back, at the center of each cell and the lamp shutter was opened and the cells were exposed to the light. Solar simulator measures I-V data within seconds. The key parameters that were taken into consideration from these measurements were short-circuit current (I_{sc}), open-circuit voltage (V_{oc}), maximum output current (I_{max}), the maximum output voltage (V_{max}), fill factor (FF), maximum out power (P_{max}). I_{sc} can be directly proportional to the number of photons that are incident on the cell. Hence, Using the I-V data, I_{sc} and P_{max} degradation rates were calculated to study the effect of encapsulant degradation on the module's performance parameters.

P_{max} and I_{sc} degradation rates were calculated using the equations (1) and (2):

$$I_{sc}\,degradation\ rate = \frac{\left(\frac{I_{sc}(pre-exposure) - I_{sc}(post-exposure)}{I_{sc}(pre-exposure)}\right) \times 100}{number\ of\ years\ of\ field\ exposure} \quad (1)$$

$$P_{max}\,degradation\ rate = \frac{\left(\frac{P_{max}(pre-exposure) - P_{max}(post-exposure)}{P_{max}(pre-exposure)}\right) \times 100}{number\ of\ years\ of\ field\ exposure} \quad (2)$$

3.3.4 Colorimetry

Colorimetry is one of the non-destructive characterization techniques used to quantify the change in color of the polymeric encapsulant material through a metric known as yellowness index (YI). The measurements were taken using an Xrite Ci-60 spectrophotometer. The instrument was calibrated using a black and a white reference. Figure 12 shows the colorimetry instrument setup. The color of discolored encapsulant ranges from light yellow to dark brown. As the color intensifies, the spectrophotometer gives a higher YI value. YI values were measured for unexposed and exposed EVA samples for comparison.

Figure 12: Colorimetry device for measuring the yellowness index

3.3.5 Thermal analytical methods

3.3.5.1 Differential Scanning Calorimetry

Differential scanning calorimetry (DSC) is one of the destructive methods used to study the phase behavior of the sample based on heat transfer during physical and chemical processes. It provides a graphical representation of heat flow (W/g) w.r.t. temperature (ºC). DSC was useful in studying various physical transition states like melting point (endothermic), crystallization point (exothermic), glass transition temperature, curing (exothermic) etc. Moreover, DSC was used to calculate the degree of crystallinity with the help of the total enthalpy method using equation (3) [19], [20]:

$$\chi_c = \frac{\Delta H_m}{\Delta H_{100}} \times 100 \qquad (3)$$

where

χ_c = degree of crystallinity

ΔH_m = specific enthalpy of melting a sample

ΔH_{100} = specific enthalpy of melting for 100% crystalline polyethylene (293 J/g) [21]

A heat-cool-heat cycle was run for EVA samples on the DSC instrument Q20 from TA instruments in a nitrogen atmosphere with a constant flow rate of 50 ml/min, shown in Figure 13. The instrument was calibrated with indium. The thermal process of the heat-cool-heat cycle is as follows [22]:

i. Ramp up from ambient temperature to 200 ºC at a heating rate of 10 ºC/min
ii. Ramp down from 200 ºC to -50 ºC at a cooling rate of 10 ºC/min
iii. Ramp up from -50 ºC to 200 ºC at a heating rate of 10 ºC/min

For sample preparation for DSC, EVA was cut using a 3/16" d hole punch and put in a low mass aluminum pan of the same diameter, followed by sealing the pan with a lid hermetically using a Tzero press. The setup for sample preparation is shown in Figure 14:

Figure 13: DSC instrument equipped with the cooling tower attachment

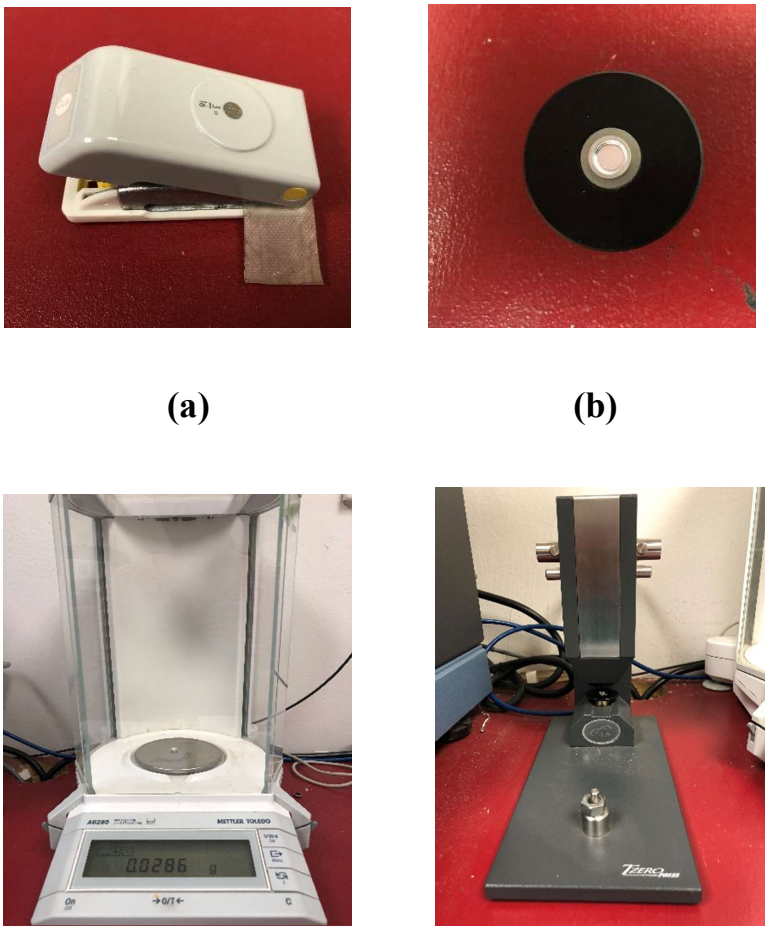

Figure 14: Equipment needed for preparing EVA samples for DSC. (a) 3/16” hole punch, (b) die for sample assembling, (c) Mettler Toledo weighing machine, and (d) Tzero press

3.3.5.2 Thermogravimetric Analysis

Thermogravimetric analysis (TGA) is also a destructive method used to study the weight change of a material w.r.t. temperature. TGA was run for the EVA samples on the Q50 TGA equipment from TA Instruments as shown in Figure 15. The purge gas was nitrogen

gas used at the flow rate of 60 ml/min. Aluminum pans were used. For EVA, the ramp-up method was used wherein the temperature was ramped up from room temperature up to 500ºC to study the thermal stability of the material. TGA was used to determine the onset points for the loss of volatile substance (acetic acid) and main chain degradation. Moreover, TGA was also used to determine the vinyl acetate content (VAc) using the equation (4) [3]:

$$VAc(\%) = \frac{HAc\ loss\ (mg) + residual\ weight\ (mg)}{Original\ weight\ (mg)} \times 100 \qquad (4)$$

where

HAc loss (mg) is the loss of acetic acid (first curve in a TGA plot)

Residual weight (mg) is the weight of vinyl acetate remaining after complete evaporation of EVA.

Original weight (mg) is the weight to be tested

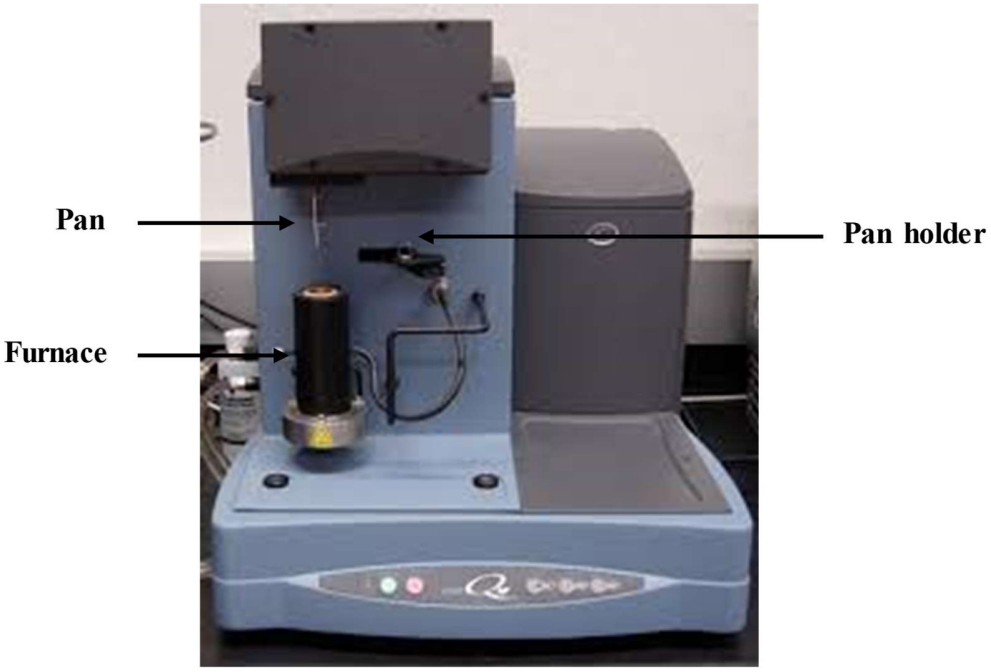

Figure 15: Experimental setup of TGA

3.3.6 Spectroscopic methods

3.3.6.1 Raman spectroscopy

Raman spectroscopy is one of the non-destructive characterization techniques used to study the molecular vibrations and crystal structures. For a molecule to be Raman active, there must be a change in its polarizability. Raman spectroscopy was used to detect fluorescence background in EVA because it becomes very intense after the aging process. Moreover, this technique was used to calculate the degree of crosslinking which happens to be one of the novel analytical methods for quantifying the crosslinking in EVA. Equation (5) was used for calculation [23][24]:

$$Crosslinking\ ratio = \frac{2941\ \text{cm-1}}{2891\ \text{cm-1}} \quad (5)$$

Where 2941 cm-1 and 2891 cm-1 correspond to CH_2 and CH_3 symmetric stretching, respectively.

The data was collected using the green laser setup with a custom-built Raman spectrometer in a 180 ° geometry. The sample was excited using a 150 mW Coherent Sapphire SF laser with a 532 nm laser wavelength. The data were collected using an Acton 300i spectrograph and a back-thinned Princeton Instruments liquid nitrogen cooled CCD detector as shown in Figure 16. The laser power was controlled using a neutral density filter wheel with an initial laser power of 100mW. The laser was focused

onto the sample using a 50X super long working distance plan APO Mitutoyo objective with a numerical aperture of 0.42. After taking the measurements, the Raman data was calibrated using cyclohexane spectrum as a reference.

Figure 16: Experimental setup for custom-built Raman system

.

3.3.6.2 Fourier Transform Infrared Spectroscopy

Fourier Transform Infrared Spectroscopy (FTIR) is a non-destructive method used to identify functional groups present in the material. For a molecule to be IR active, there must be a change in its dipole moment. FTIR was used to detect the presence of degradation products formed in EVA caused by the chemical reactions leading to its degradation.

FTIR measurements were taken using the 4300 Agilent handheld FTIR as shown in Figure 18, to investigate any functional group changes in the EVA encapsulant after being aged due to its field exposure. Instead of using the transmission mode, measurements were taken using Diamond-Attenuated Total Reflectance (D-ATR) FTIR working on the principle of total internal reflection. Unlike the transmission

mode, the IR radiation does not penetrate the whole sample in D-ATR. It is totally reflected after penetrating a certain depth of the sample in contact with the diamond. The reason for using D-ATR method is that EVA is a thick material because of which the radiation is completely absorbed before passing through it which results in noisy peaks in the spectrum. For the D-ATR FTIR method, the sample is brought in contact with the diamond to get the FTIR spectrum. FTIR measures spectra in the mid-IR wavelength range (4000 cm^{-1} to 400 cm^{-1}). Figure 17 gives the mechanism of D-ATR FTIR.

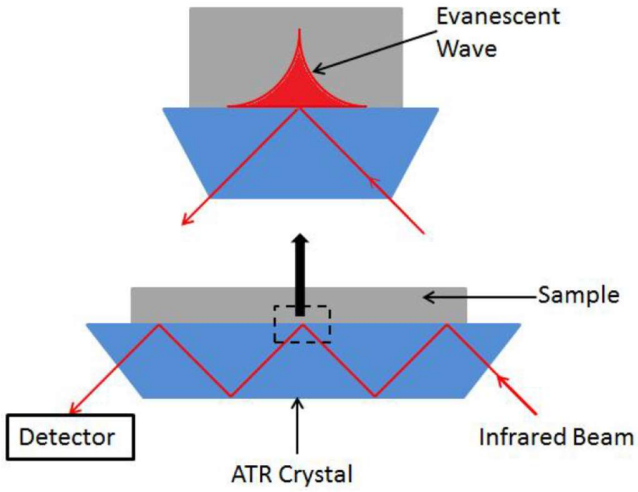

Figure 17: Overview of the Diamond-ATR FTIR mechanism [25]

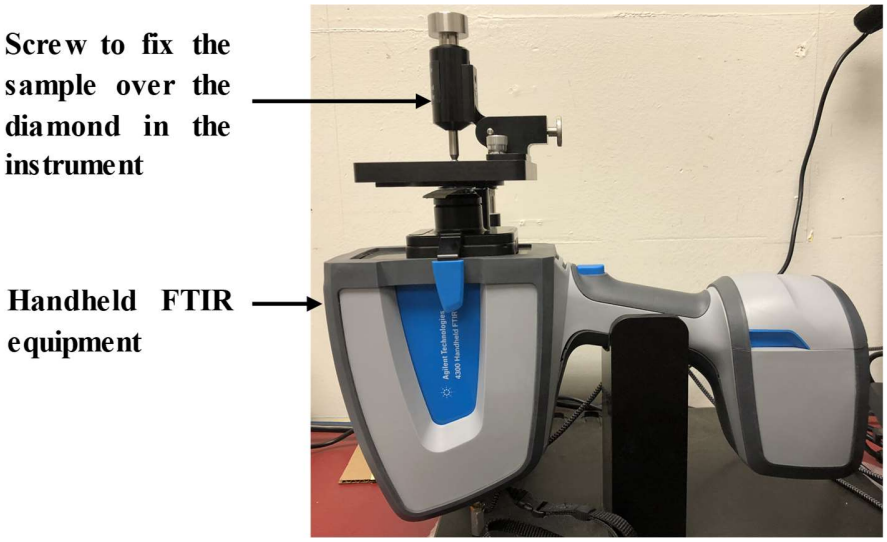

Figure 18: Experimental setup for handheld FTIR

4. RESULTS AND DISCUSSION

4.1 Visual inspection

Under visual inspection, module type I and II showed browning at the center of the cells whereas the edges and non-cell regions showed little yellowing. Instead, the edges were translucent indicating occurrence of photobleaching. However, module type III showed prominent discoloration of the encapsulant over the whole cell area (center and edge) as well as the non-cell area. It is because of restricted moisture ingression and oxygen penetration in the glass/glass module, and hence no photobleaching. Figure 19 shows the visual images of modules type I, II and III.

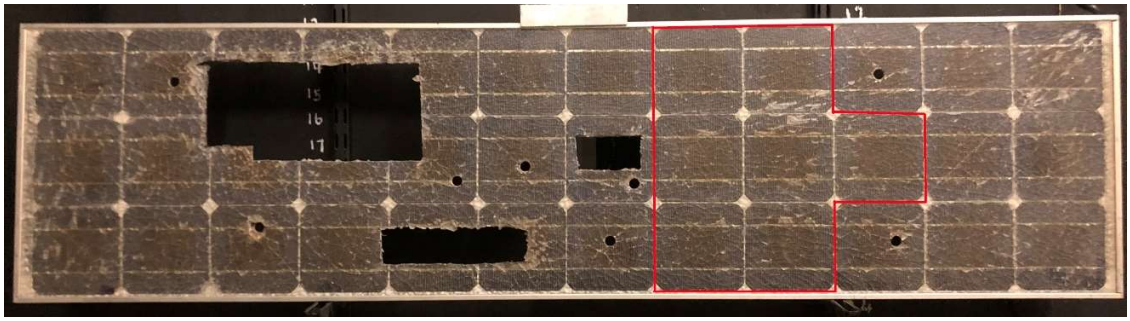

(a)

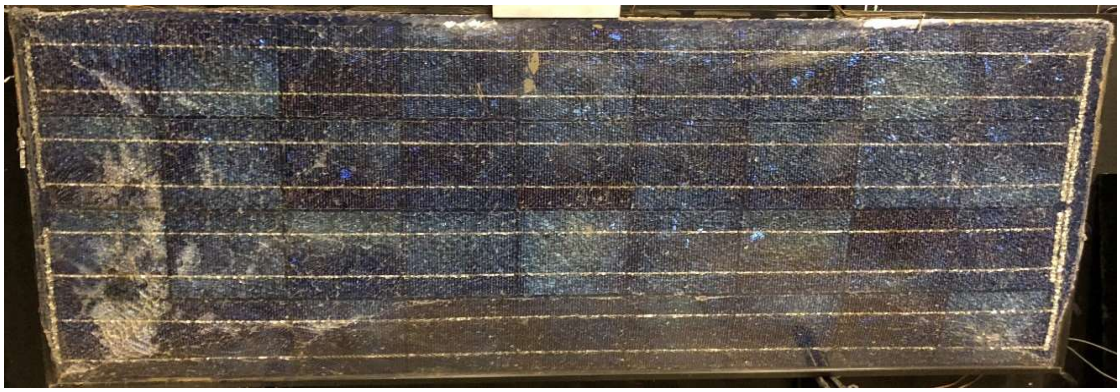

(b)

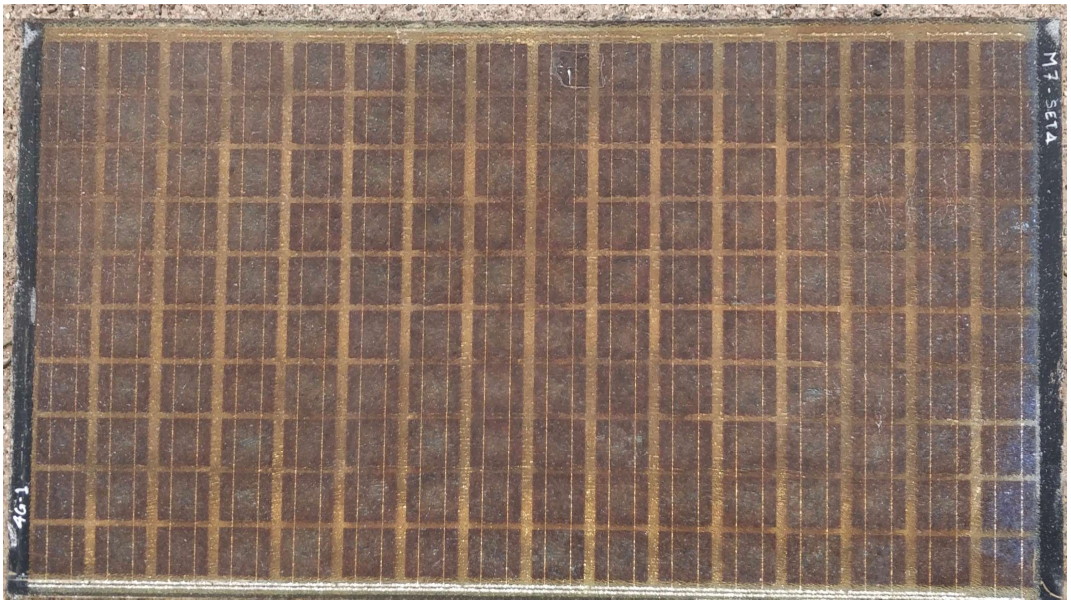

(c)

Figure 19: Visual images of (a) module type I (glass/backsheet) (b) module type II (glass/backsheet) and (c) module type III (glass/glass)

4.2 Discoloration area from UV fluorescence imaging

Using UV fluorescence imaging, it is easier to mark the exact area of browning in the encapsulant which is difficult by visual inspection unless the browning is prominent. Figure 20 shows the UVF images of modules type I, II and III.

For glass/backsheet module type I (Figure 20 (a)) and type II (Figure 20 (b)), prominent discoloration of the encapsulant is observed at the cell centers. However, module type I

shows browning along and beyond the cell interconnects regions whereas module type II has discoloration contained within the interconnect region. Another difference between these two modules is the uniformity of browning throughout the modules. Module type I shows almost uniform browning at the centers whereas module type II shows non-uniformity in browning at the centers throughout the module. The reason could be that in module type II, the adhesion between the layers could have weakened causing more moisture/oxygen ingression and thus causing a higher amount of photobleaching. Moreover, the cells in module type II had many cracks which could have increased the oxygen ingression causing more photobleaching. Also, no discoloration is observed at the cell edges and the non-cell regions of both the modules indicating that these areas are photobleached. However, the glare observed in the images is because of the glare from the UV torches and not to be mistaken as browning.

For module type III (Figure 20 (c)), discoloration is intensified over the whole module including the cell centers, edges, and the non-cell regions.

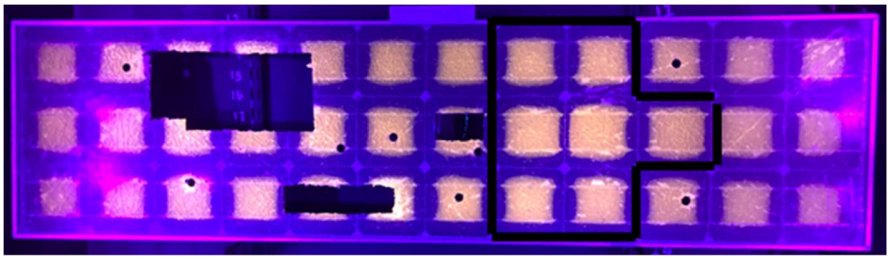

(a)

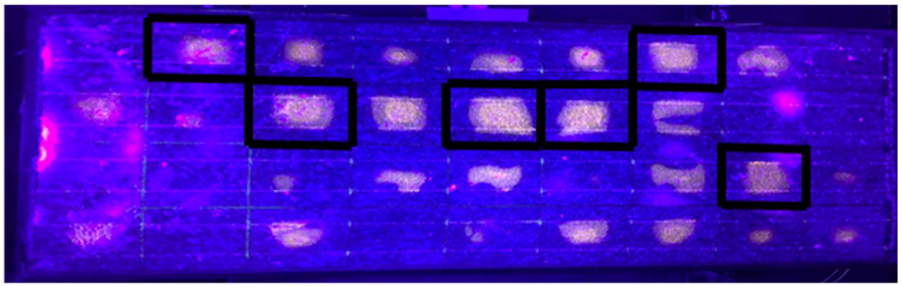

(b)

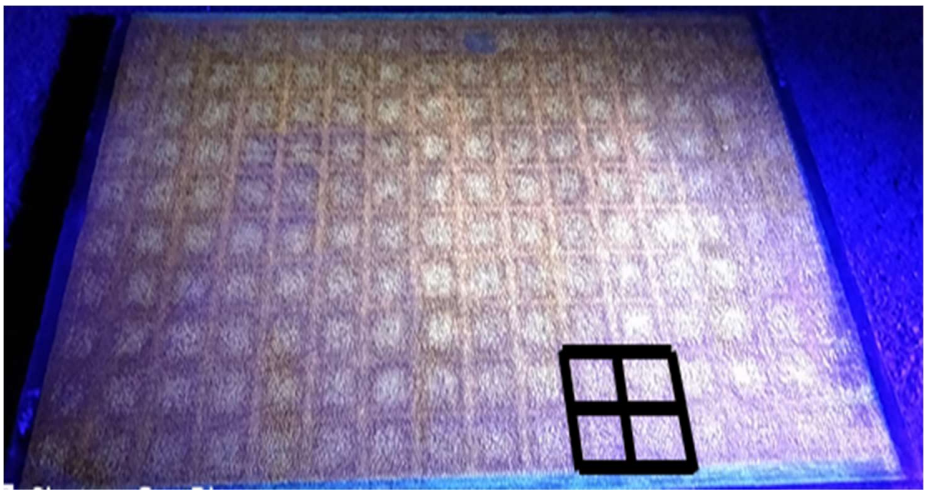

(c)

Figure 20: UV fluorescence images of (a) module type I (b) module type II and (c) module type III. Marked cells are the extracted cells for investigation.

In case of glass/backsheet modules, it is quite noticeable that module type I has higher browning because it is not as photobleached as module type II. This could be because of longer field exposure which might have caused higher moisture/oxygen ingression through the backsheet.

When glass/backsheet modules (type I and II) are compared with the glass/glass module (type III), it is evident that glass/glass module did not have any oxygen ingression because of which no part of the encapsulant is photobleached. Instead, the browning is more prominent in type III compared to type I and II. The reason could be because the glass/glass modules are hermetically sealed which does not allow oxygen to penetrate through unlike the case in glass/backsheet modules where the oxygen transmission rate of backsheet increases with increase in its degradation.

Cell samples were extracted as per the method explained in section 3.2 after analyzing the visual and UVF images.

4.3 Estimation of I_{sc} and P_{max} degradation rates from I-V measurement

Encapsulant degradation directly affects the performance parameters of the module. Discoloration of EVA encapsulant reduces the transmission of light which causes a decrease in the efficiency of the module. Current and power degradation rates were calculated using equations (1) and (2), respectively. Table 2 and Table 3 show the calculated values for I_{sc} and P_{max} degradation rates, respectively. For (I_{sc}, P_{max}) degradation rates (%/year), the trend for the modules is: type III (1.46, 2.28) > type I (0.41, 1.01) > type II (0.29, 0.44). It is evident that the degradation rates for module type III are higher than the module types I and II. The reason for this difference could be the difference in the extent of EVA degradation in glass/backsheet and glass/glass modules. Another

observation that can be drawn from the results is that the ratio of I_{sc} loss to P_{max} loss indicates that the majority of power loss is due to the encapsulant discoloration.

Table 2: Calculation of I_{sc} degradation rates per pear for modules type I, II, and III

Effect of degradation on I_{sc} (A)			
	Module type I (glass/backsheet)	Module type II (glass/backsheet)	Module type III (glass/glass)
I_{sc} pre-exposure (A) (nameplate reading)	3.35	3.89	4.95
I_{sc} post- exposure (A)	3.101	3.65	4.225
I_{sc} degradation (%)	7.43	6.17	14.65
Years of exposure	18	21	10
I_{sc} degradation rate (%/year)	0.41	0.29	1.46

Table 3: Calculation of P_{max} degradation rates per pear for modules type I, II, and III

Effect of degradation on P_{max} (W)			
	Module type I (glass/backsheet)	Module type II (glass/backsheet)	Module type III (glass/glass)
P_{max} pre-exposure (W) (nameplate reading)	53	62.5	300

P_{max} post- exposure (W)	43.4	56.70	231.60
P_{max} degradation (%)	18.11	9.28	22.80
Years of exposure	18	21	10
P_{max} degradation rate (%/year)	1.01	0.44	2.28

4.4 Quantification of Encapsulant Browning

Figure 21 shows the yellowness indices for unexposed EVA and cell samples of module types I, II and III.

When compared on the same scale, EVA from module type III show the highest values of YI. Whereas, cells from module type I show higher values of YI compared to that from module type II. Hence, the YI has a following trend for the modules: type III > type I > type II. When compared among the edges, centers, and non-cell regions, module type III has the following trend for YI: non-cell > edges > centers. However, for module type I, the trend is: centers > edges > non-cell and for module type II, the trend is: centers > non-cell > edges.

Since the cells operate at a slightly higher temperature than the non-cell regions, EVA from the cell regions, especially the cell center regions are bound to have higher browning compared to the non-cell regions which is a trend followed by the glass/backsheet modules (type I and II). But in glass/backsheet modules, photobleaching takes place due to moisture/oxygen ingression causing the yellow regions to turn translucent white due to

oxidation of polyene chains. Therefore, in glass/backsheet molecules (type I and II), the YI values for non-cell EVA are close to but slightly higher than the unexposed EVA due to degradation. Moreover, backsheet helps in diffusing out the acetic acid produced and hence, helps in preventing additional catalytic degradation caused by acetic acid. Whereas, glass/glass module (type III) is hermetically sealed because of which acetic acid cannot be diffused out through either the module edges or the backsheet. Thus, it gets entrapped and accelerates the degradation. Besides, non-cell EVA is double layered consisting of the front as well as back EVA which causes a higher amount of acetic acid production causing higher discoloration in that region. Also, since acetic acid follows a pathway through cells to non-cell regions to escape through the module edges, it is difficult for acetic acid to diffuse out because of the module being tightly sealed. This again causes yellowing to darken in the non-cell region caused by the escaping acetic acid entrapped there. Therefore, non-cell EVA shows the highest YI followed by the cell edges and then the cell centers having the least YI.

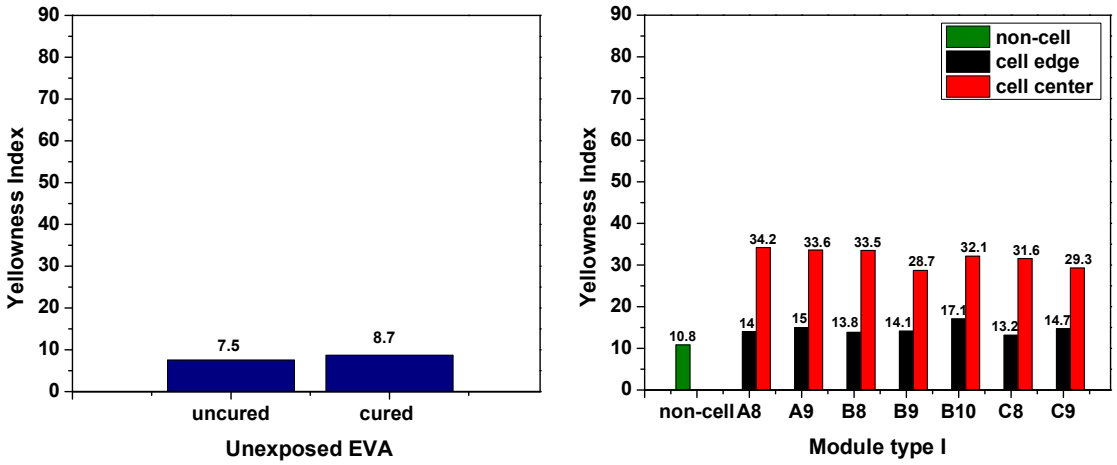

(a) **(b)**

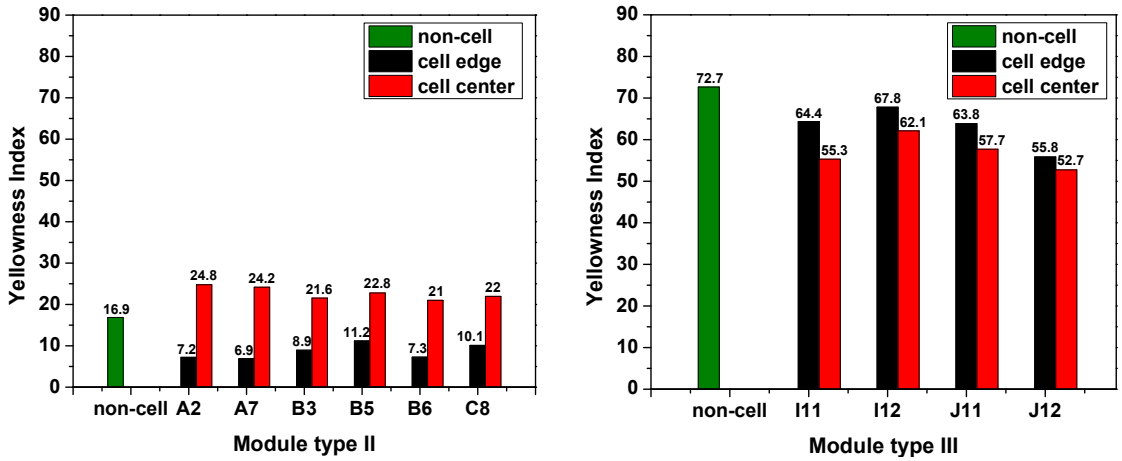

(c) **(d)**

Figure 21: Yellowness indices for (a) unexposed EVA, EVA samples from (b) module type I, (c) module type II, and (d) module type III

4.5 Determination of degree of crystallinity from DSC

Figure 22 shows the typical DSC trend for EVA. DSC provides a graph of heat flow (W/g) vs. temperature (ºC). The phase behavior of EVA is generally studied within temperature range -50 ºC to 200 ºC. Since we run the heat-cool-heat cycle, the run begins by heating the sample from room temperature (25-30 ºC) to 200 ºC at a certain heating rate. During the first heating, we get two melting peaks in the temperature range of 50-70 ºC. These double peaks correspond to the crystal melting. The first melting peak corresponds to the melting of the imperfect crystalline phase of EVA whereas the second melting peak corresponds to the melting of perfect crystalline phase present in EVA because of more the crystallinity, higher the melting point. The area under the curve gives the latent heats of fusion. As we continue heating up to 150 ºC, an exothermic peak is seen which denotes the

process of curing. The area under that curve can be directly related to the amount of curing agent present in EVA before curing.

On cooling down to -50 ºC, an exothermic curve is obtained which corresponds to the re-crystallization of EVA. The area under this re-crystallization curve gives heat released for this process. When the material is heated at a constant heating rate, a step change in the plot is visible at around -35 to 40 ºC corresponding to the glass transition temperature of EVA indicating a change in specific heat capacity. During the second heating, one of the two melting peaks disappears due to the fact that the structure of the material has changed. Instead of a peak, it gives a broad curve indicating the presence of imperfect crystallites of different sizes. Apparently, the crystallization process was not fast enough to reform the perfect original crystalline phase of the material.

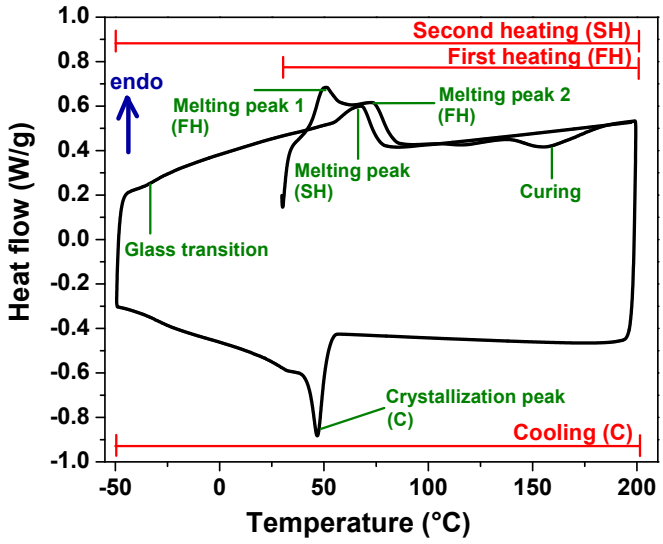

Figure 22: Typical DSC plot for EVA copolymer

Figure 23 and Figure 24, Figure 25, Figure 26 show the DSC plots for unexposed and field-aged cell samples of modules type I, II, and III, respectively. All the DSC plots have exo-down orientation. For all three modules, one case of the non-cell region and another case of edge and center regions of EVA extracted from one of the selected cells is shown below. The remaining DSC plots are given in Appendices A.1., B.1., and C.1.

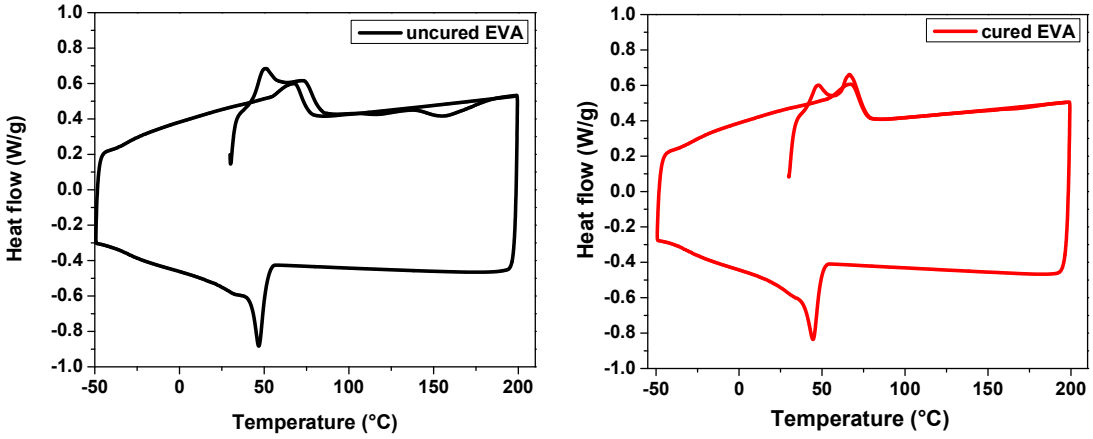

(a) **(b)**

Figure 23: DSC plots for unexposed (a) uncured, and (b) cured EVA

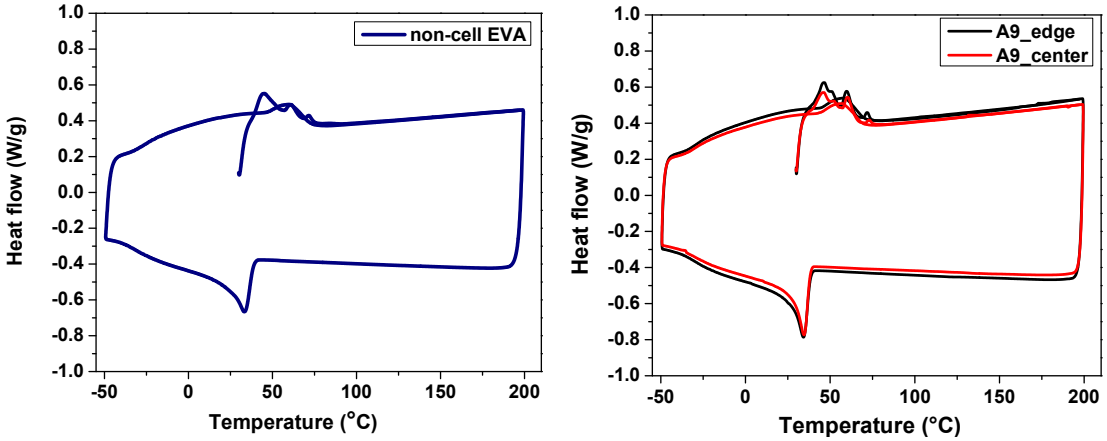

(a) **(b)**

Figure 24: DSC plots for field exposed (a) non-cell EVA, and (b) edge and center EVA from module type I

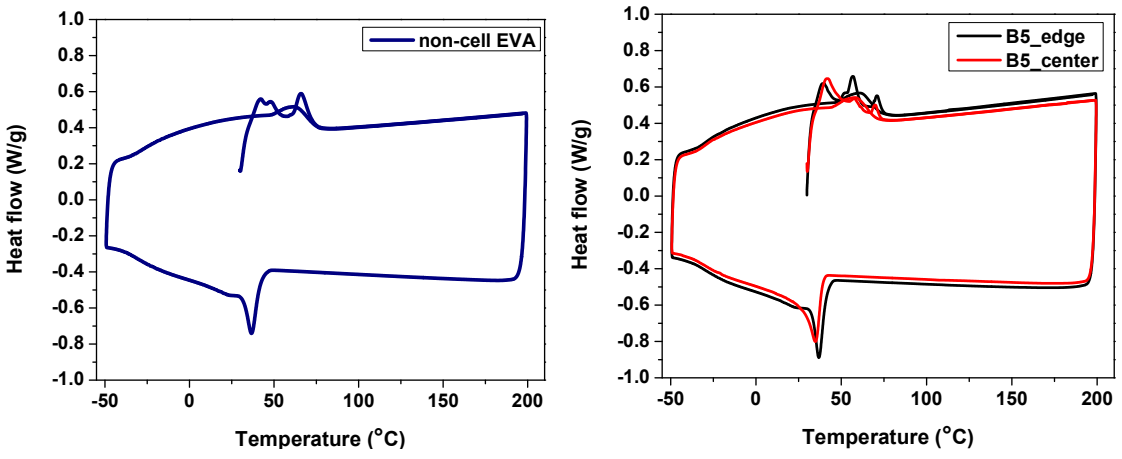

(a) **(b)**

Figure 25: DSC plots for field exposed (a) non-cell EVA, and (b) edge and center EVA from module type II

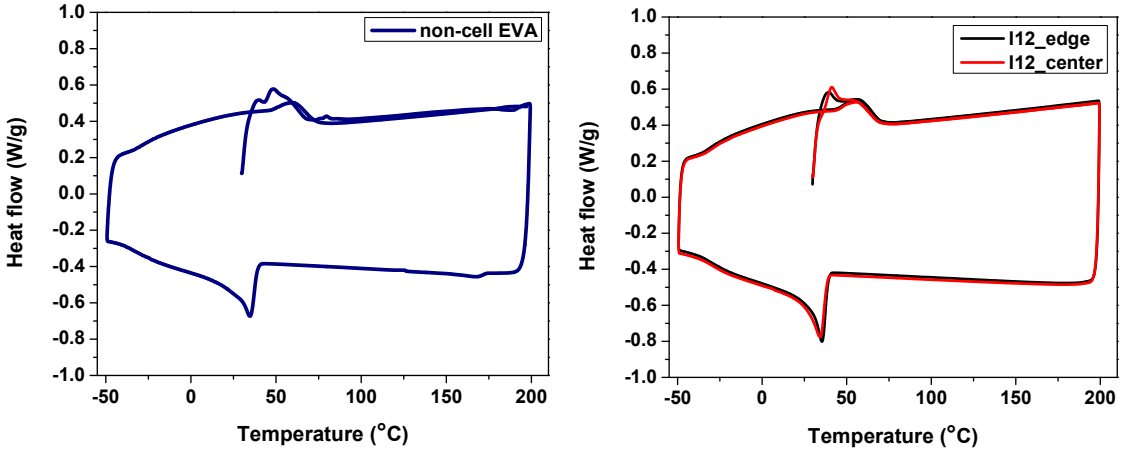

(a) **(b)**

Figure 26: DSC plots for field exposed (a) non-cell EVA, and (b) edge and center EVA from module type III

From the DSC plots, it is evident that the module types I and II have a significant third melting endotherm. It simply corresponds to a broad range of sizes of imperfect and perfect crystallites present in the EVA.

The degree of crystallinity is calculated by using equation (3) which calculates the area under the melting curves of first heating because the second heating may not give the accurate degree of crystallinity due to the removal of thermal history from first heating. Also, in the second heating, the melting curve for perfect crystallites disappear. Figure 27 shows the graphical representation of the degree of crystallinity of EVA samples. Type I and II (Glass/backsheet) modules have the following order for the degree of crystallinity in decreasing order: uncured > cured > non-cell > cell edges > cell centers. Whereas, type III (glass/glass) module has the following order for the degree of crystallinity in decreasing order: uncured > cured > cell centers> cell edges > non-cell. This could be because of the fact that UV rays and temperature distort the original structure of EVA causing chemical reactions to occur resulting into formation of volatile products. This either restricts or decreases the degree of crystallinity in the copolymer because of the presence of many non-crystallites after distortion.

Another observation is that the order of degree of crystallinity reverses for cell samples in type III module. This could be because of entrapment of acetic acid along with the production of acetic acid and other volatile products in the non-cell region and since that

region has double layered EVA, production of acetic acid will be higher leading to decrease in crystallinity.

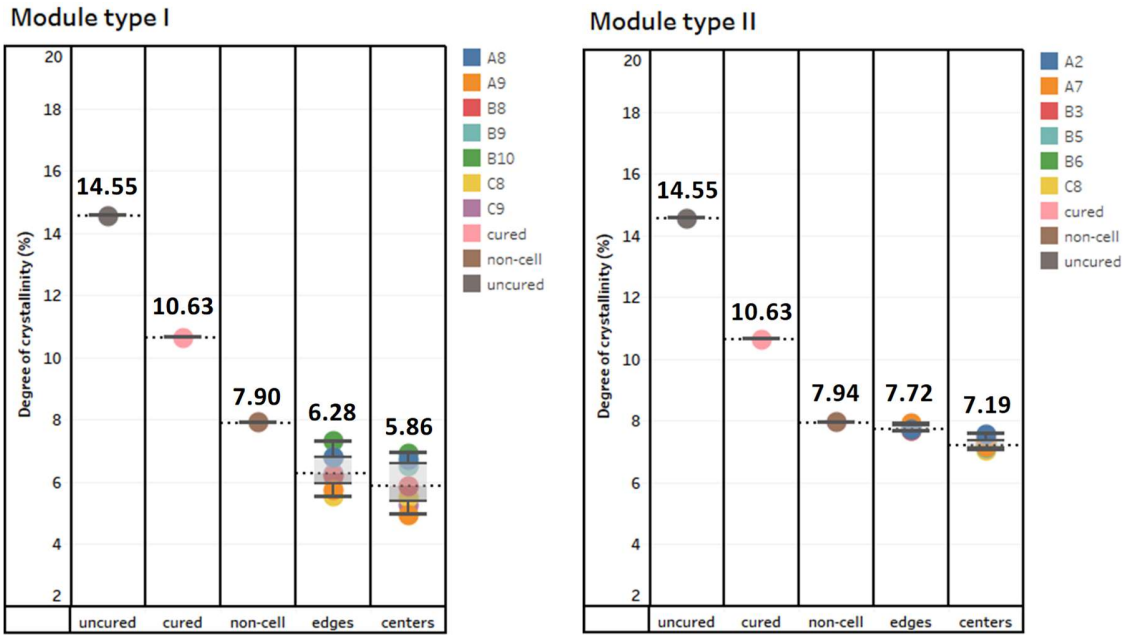

(a) **(b)**

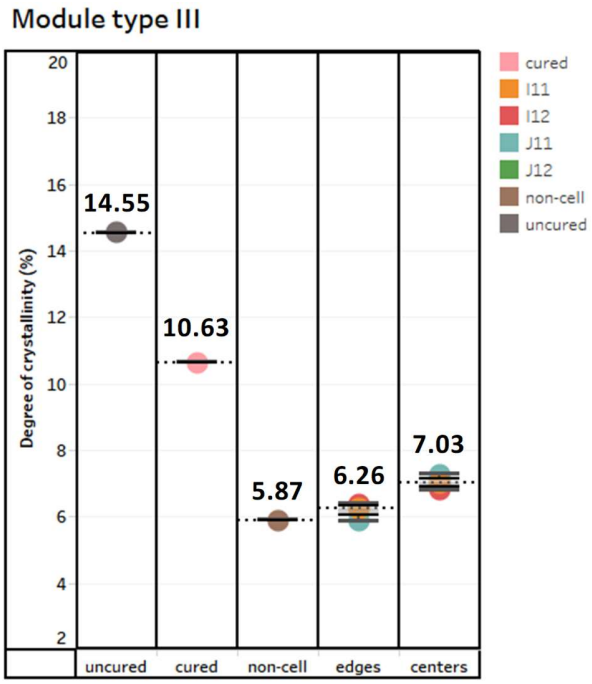

(c)

Figure 27: Graphical representation of the degree of crystallinity for (a) module type I, (b) module type II, and (c) module type III

4.6 Calculation of vinyl acetate content (VAc) from TGA

Figure 28 shows the typical TGA trend for EVA. It shows the non-isothermal TGA profile for EVA. As EVA is exposed to higher temperatures in a nitrogen atmosphere, the first to melt at~320ºC is the volatile compound i.e. acetic acid produced by deacetylation reaction (Norrish II reaction) caused in the vinyl acetate group in EVA. This is followed by the main chain breakdown (polyethylene) at~430ºC.

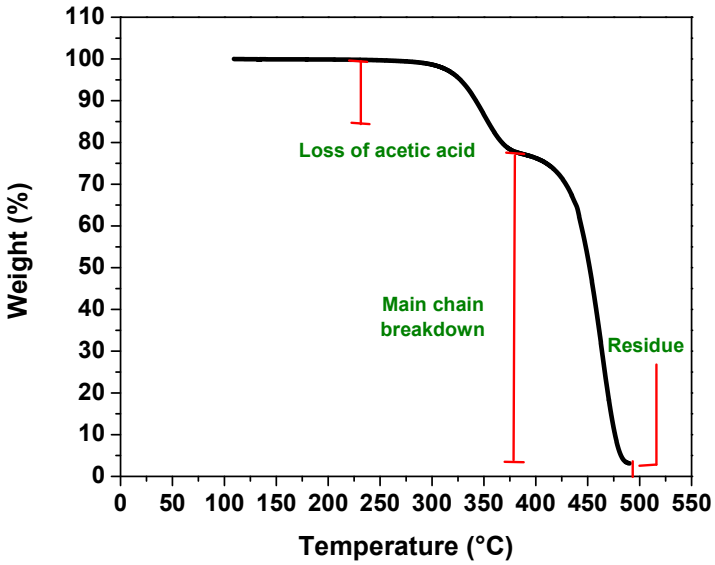

Figure 28: Typical TGA plot for EVA

Figure 29 and Figure 30, Figure 31, Figure 32 show the TGA plots for unexposed and field-aged cell samples of modules type I, II, and III, respectively. For all three modules, one case of the non-cell region and another case of edge and center regions of EVA extracted from one of the selected cells is shown below. The remaining TGA plots are given in Appendices A.2., B.2., and C.2.

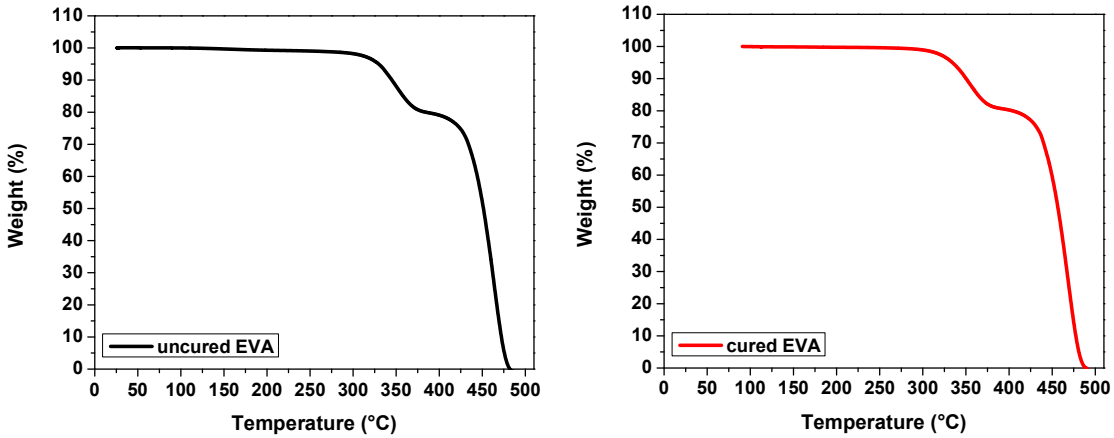

(a) **(b)**

Figure 29: TGA plots for unexposed (a) uncured, and (b) cured EVA

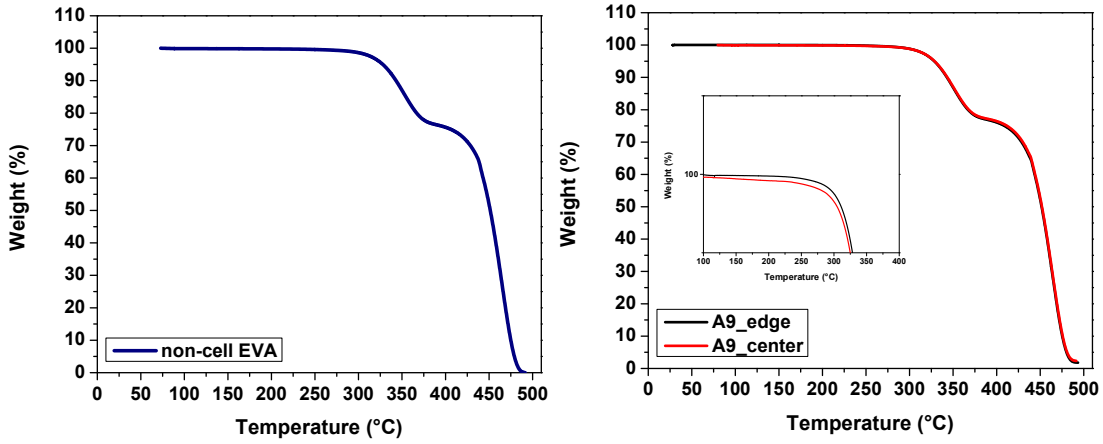

(a) **(b)**

Figure 30: TGA plots for field exposed (a) non-cell EVA, and (b) edge and center EVA from module type I

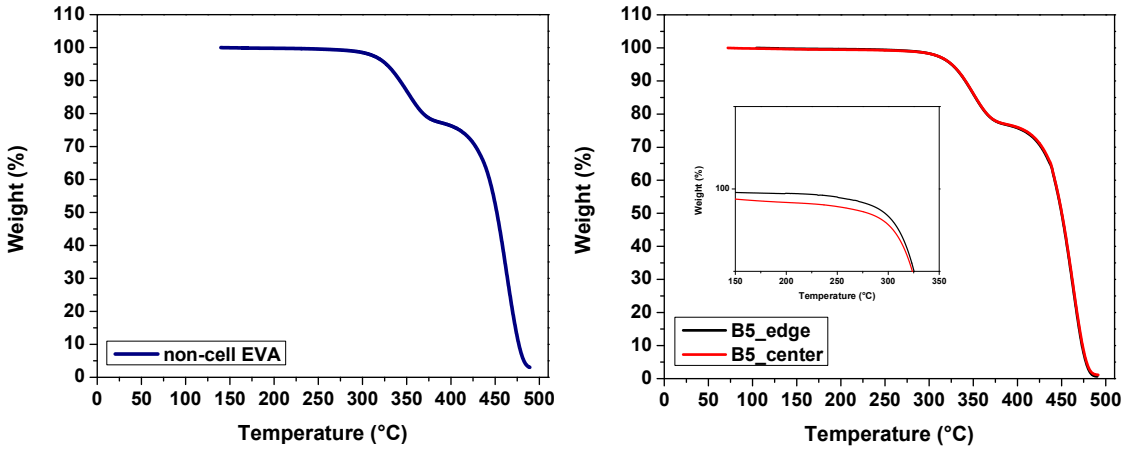

(a) **(b)**

Figure 31: TGA plots for field exposed (a) non-cell EVA, and (b) edge and center EVA from module type II

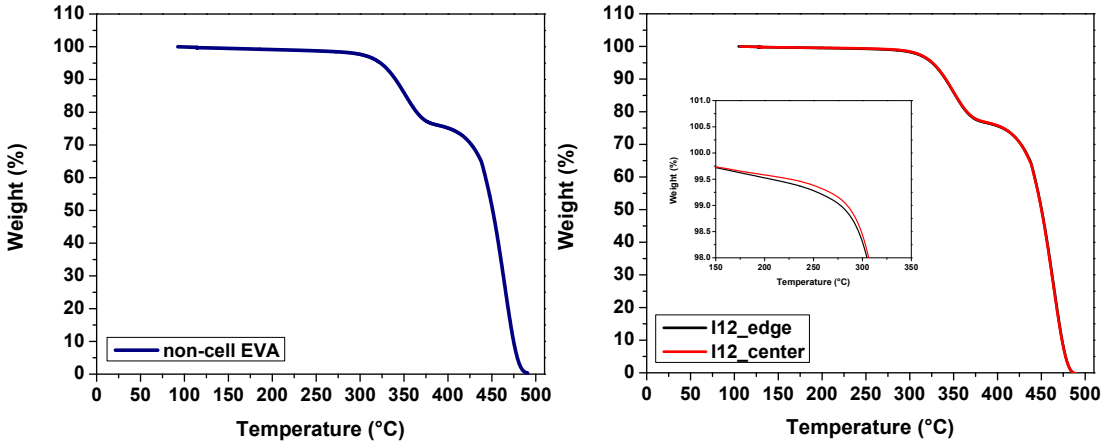

(a) **(b)**

Figure 32: TGA plots for field exposed (a) non-cell EVA, and (b) edge and center EVA from module type III

It is evident that in modules type I and II, EVA from cell centers have lower onset temperatures for the evolution of acetic acid compared to the cell edges whereas, in type III module, cell center EVA has higher onset temperature than cell edge EVA. Thus, EVA from cell edges is said to have higher thermal stability than that from cell centers for glass/backsheet modules whereas the trend reverses in case of glass/glass module. This could be because of double the thickness of EVA in non-cell regions and absence of moisture/oxygen ingression in those respective regions causing an increase in the rate of deacetylation reaction in module type III.

Vinyl acetate content (VAc) is calculated using the data obtained from TGA data using equation (4). The vinyl acetate that was consumed in the production of acetic acid evaporates followed by degradation of polyethylene. Hence, the residue is considered as the leftover vinyl acetate in the sample because of which it is considered while calculating VA content.

Figure 33 shows the graphical representation of the vinyl acetate content calculated for the EVA samples. Type I and II (Glass/backsheet) modules have the following order for vinyl acetate content in decreasing order: cell centers > cell edges > non-cell > cured > uncured. Whereas, type III (glass/glass) module has the following order for vinyl acetate content in decreasing order: non-cell > cell edges > cell centers> cured > uncured. The change in thermal stability could be because of the change in crystallinity of the material. Due to atmospheric thermal cycles, crystallinity could have caused structural changes which resulted in a change in thermal stability as well as in VA content in EVA.

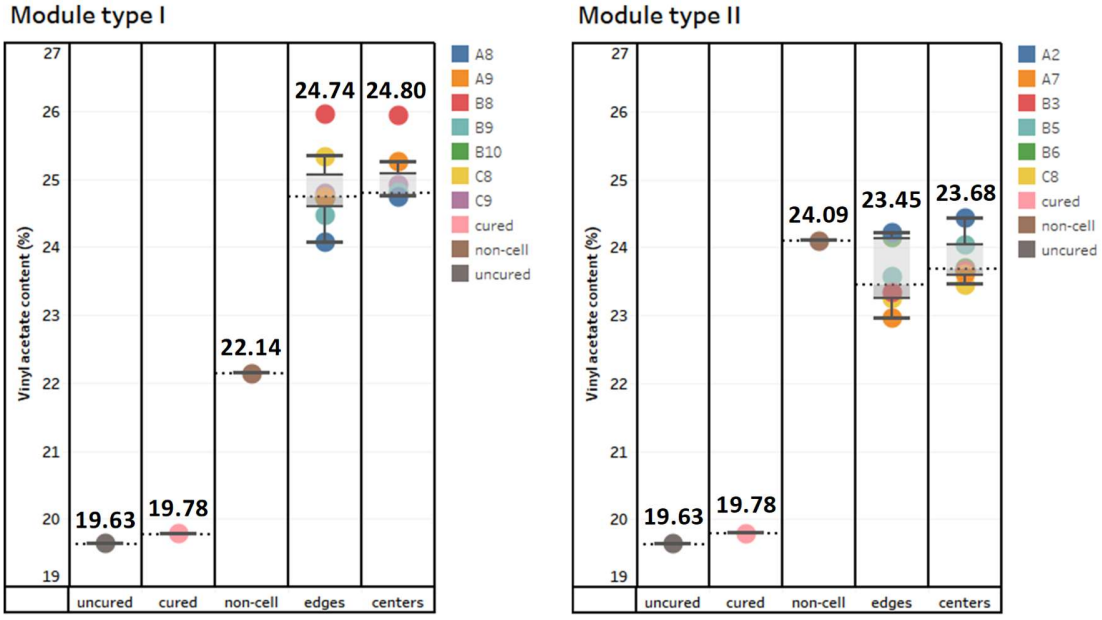

(a) **(b)**

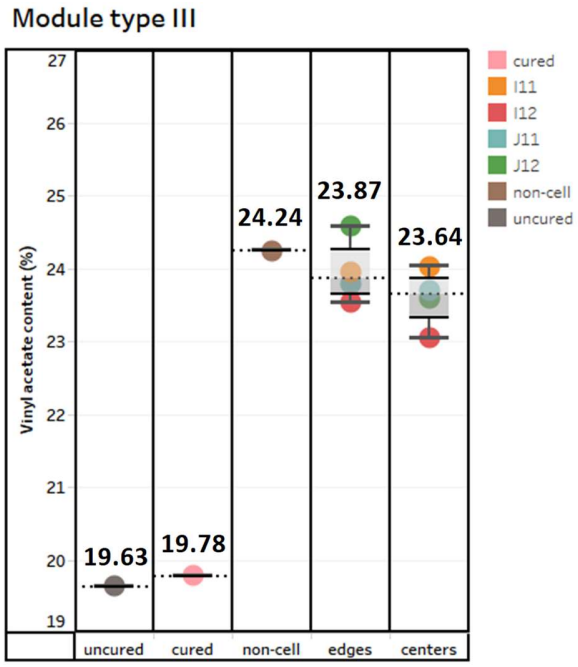

(c)

Figure 33: Graphical representation of vinyl acetate content (VAc) for (a) module type I, (b) module type II, and (c) module type III

4.7 Estimation of the degree of crosslinking from Raman spectra

Figure 34 shows the typical Raman trend for EVA with the characterization peaks to the functional groups of the compounds present in the tested sample.

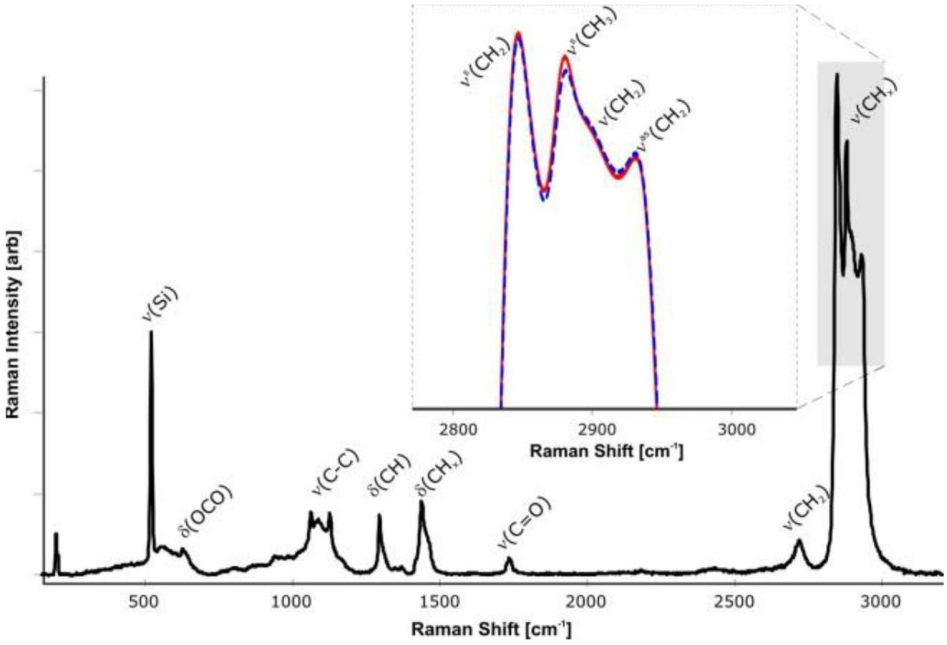

Figure 34: Typical Raman plot for EVA [26]

Figure 35, and Figure 36, Figure 37, Figure 38 show the Raman plots for unexposed and field-aged cell samples. For all three modules, one case of the non-cell region and another case of edge and center regions of EVA extracted from one of the selected cells is shown below. The remaining Raman plots are given in Appendices A.3., B.3., and C.3.

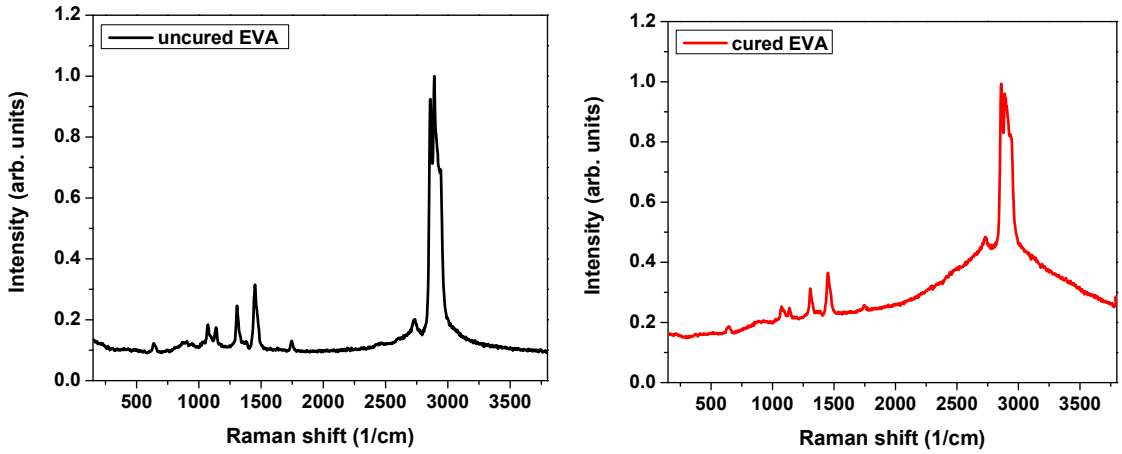

(a) **(b)**

Figure 35: Raman plots for unexposed (a) uncured, and (b) cured EVA

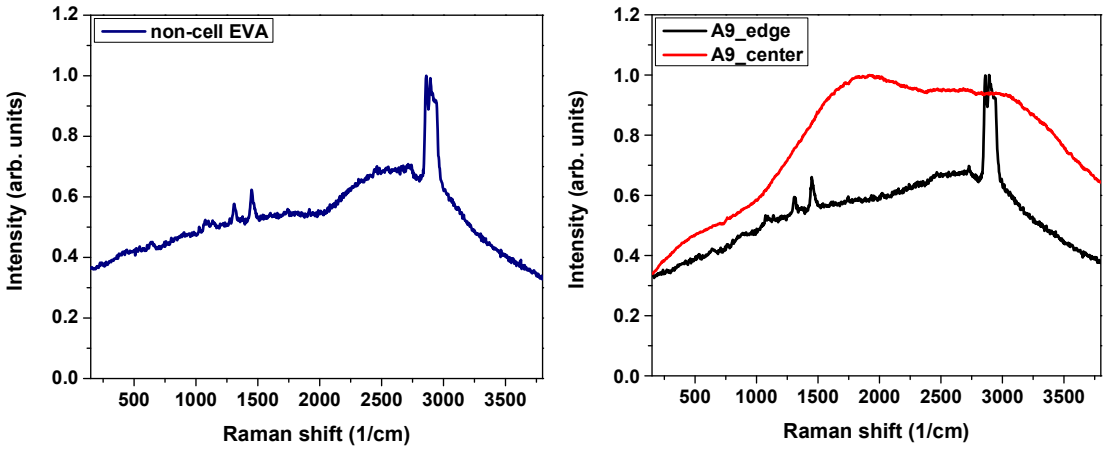

(a) **(b)**

Figure 36: Raman plots for field exposed (a) non-cell EVA, and (b) edge and center EVA from module type I

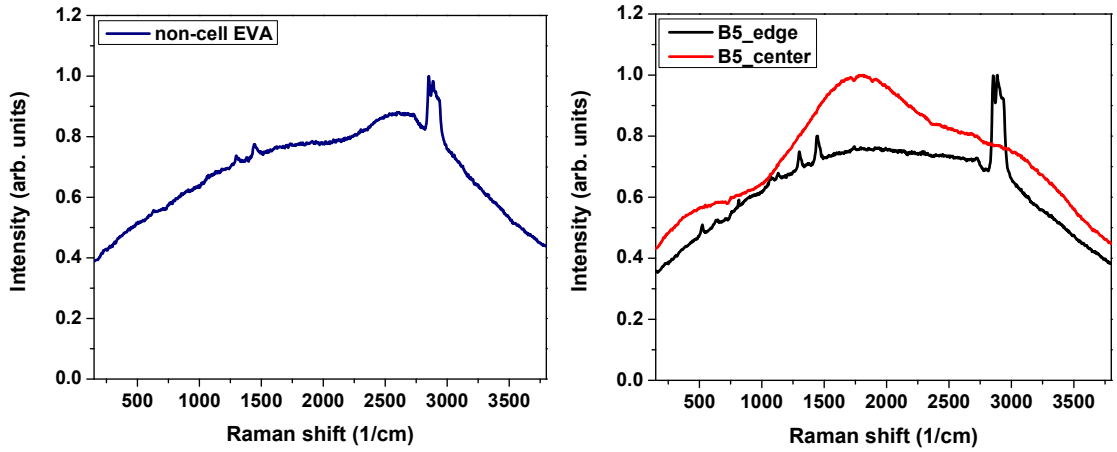

(a) **(b)**

Figure 37: Raman plots for field exposed (a) non-cell EVA, and (b) edge and center EVA from module type II

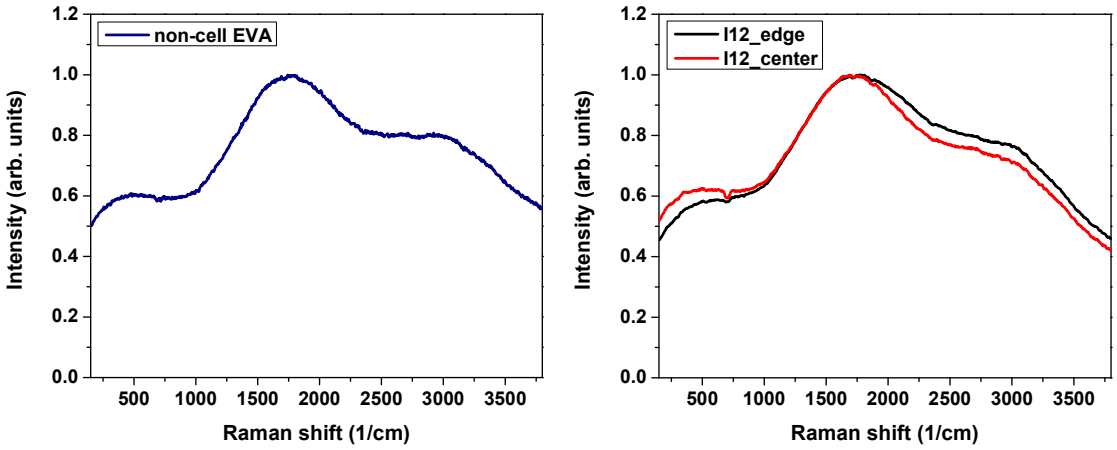

(a) **(b)**

Figure 38: Raman plots for field exposed (a) non-cell EVA, and (b) edge and center EVA from module type III

In Raman spectroscopy, polyenes produced as a result of Norrish II reaction causes an increase in the fluorescence background and change in intensity of EVA peaks in Raman spectra [14]. From the Raman spectra of EVA samples, it is evident that in modules type I and II, centers have higher fluorescence background and disappearing Raman peaks indicating higher degradation of centers compared to the edges. However, for module type III, fluorescence background is in the following decreasing order: non-cell > cell edges > cell centers.

During the process of crosslinking, CH_3 terminal groups of vinyl acetate take part in a radical reaction wherein CH_3 groups are transformed into CH_2 bridges [23]. Hence, the

degree of crosslinking is calculated by taking the ratio of symmetric vibrations of CH_2 and CH_3 groups i.e. using equation (5).

Figure 39 shows the graphical representation of the degree of crosslinking for EVA samples. Module type I has the following order for the degree of crosslinking in decreasing order: cell centers > cell edges > non-cell > cured > uncured. Module type II has the following order for the degree of crosslinking in decreasing order: cell centers > non-cell > cell edges > cured > uncured. However, module type III has the following order for the degree of crosslinking in decreasing order: non-cell > cell edges > cell centers > cured > uncured. There is a possibility that the thickness of the EVA, the spacing of the cells and absence of oxygen can be some of the factors leading to the change in the degree of crosslinking between glass/backsheet and glass/glass modules.

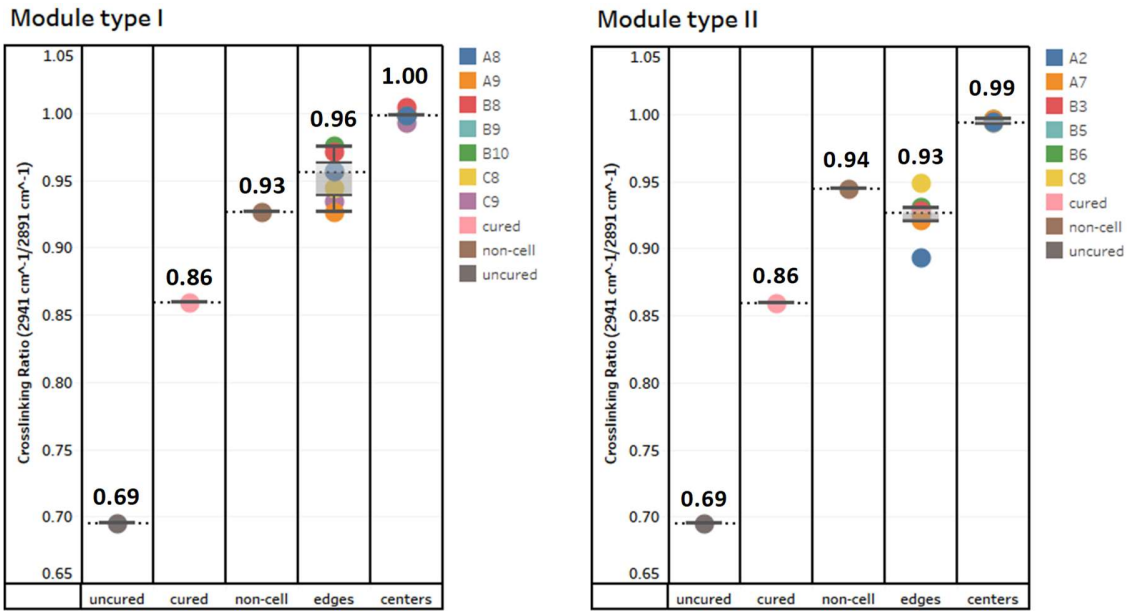

(a) **(b)**

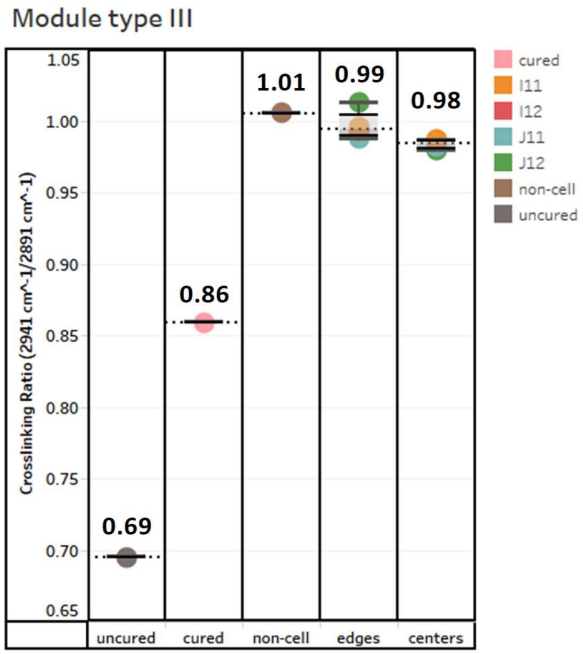

(c)

Figure 39: Graphical representation of crosslinking ratio for (a) module type I, (b) module type II, and (c) module type III

4.8 Presence of degradation products

Figure 40 shows the typical FTIR trend for EVA. It shows the peaks for EVA copolymer. The peaks at which the functional groups are labeled in red and green correspond to the FTIR peaks for polyethylene and vinyl acetate, respectively. The intensity of the peak can be related to the extent of the functional group present in the sample.

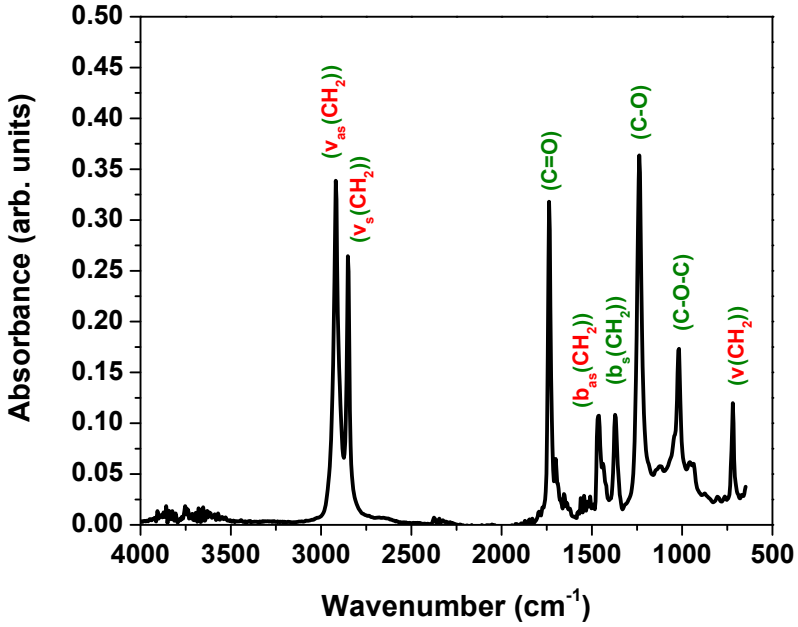

Figure 40: Typical FTIR plot for EVA

Figure 41, and Figure 42, Figure 43, Figure 44 show the FTIR plots for unexposed and field-aged cell samples. For all three modules, one case of the non-cell region and another case of edge and center regions of EVA extracted from one of the selected cells is shown below. The remaining Raman plots are given in Appendices A.4., B.4., and C.4.

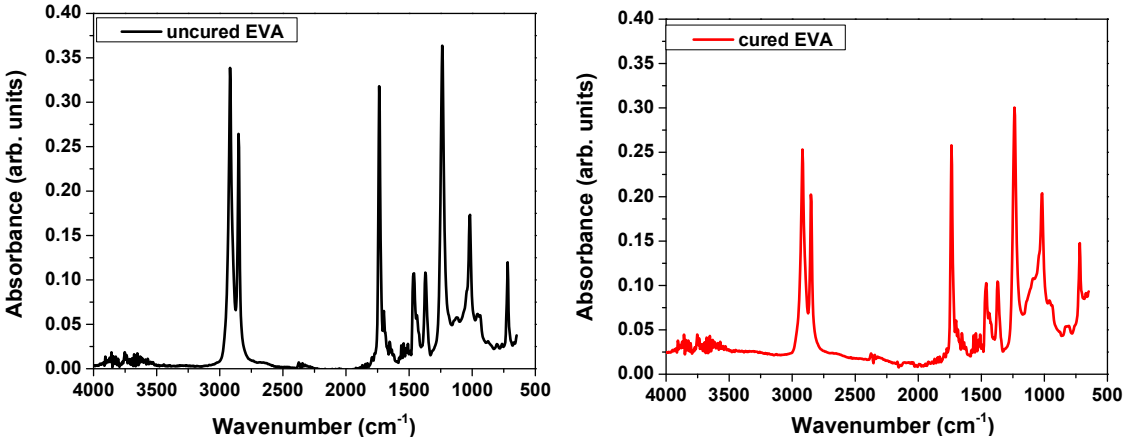

(a) **(b)**

Figure 41: FTIR plots for unexposed (a) uncured, and (b) cured EVA

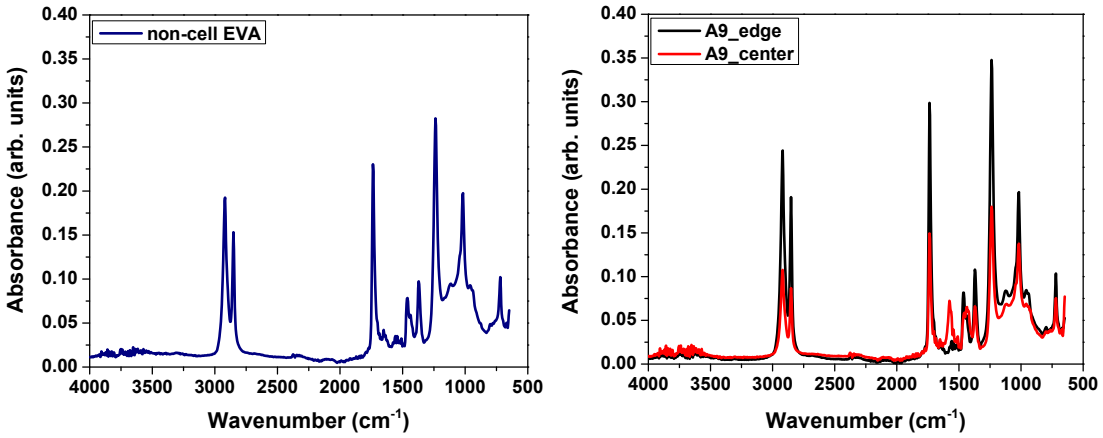

(a) **(b)**

Figure 42: FTIR plots for field exposed (a) non-cell EVA, and (b) edge and center EVA from module type I

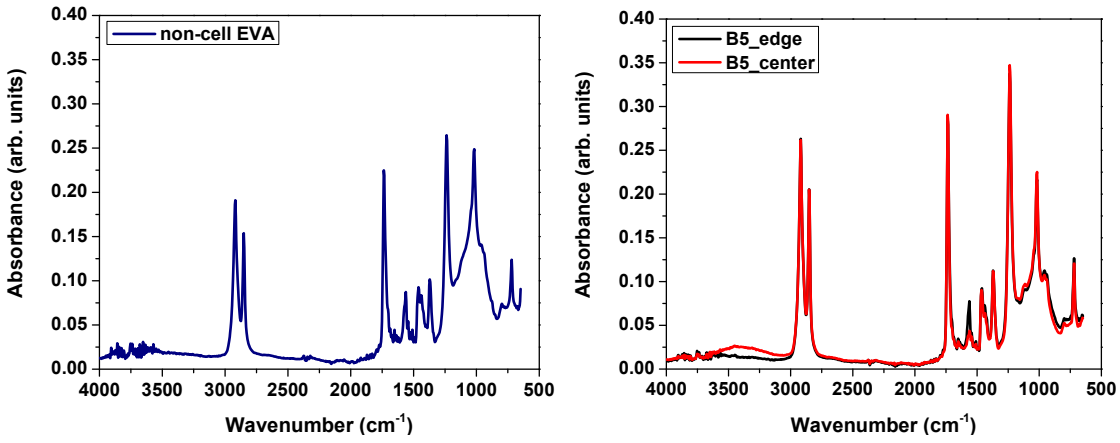

(a) **(b)**

Figure 43: FTIR plots for field exposed (a) non-cell EVA, and (b) edge and center EVA from module type II

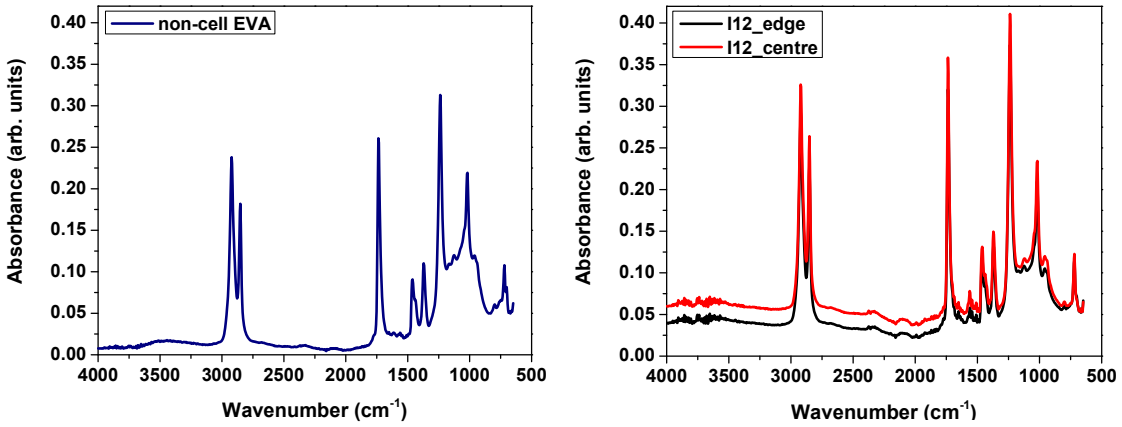

(a) **(b)**

Figure 44: FTIR plots for field exposed (a) non-cell EVA, and (b) edge and center EVA from module type III

From the FTIR plots, it is evident that there have been chemical changes in the EVA samples from the three modules. Since FTIR helps in monitoring the presence of any degradation products formed due to chemical reactions, these peaks are compiled in Table 4, Table 5 and Table 6 for module type I, II, and III, respectively. The red peaks correspond to that of polyethylene and the blue peaks correspond to that of vinyl acetate. EVA from all three modules shows the presence of polyenes (C=C) and allylic unsaturation. This confirms the occurrence of the Norrish II reaction which causes the formation of polyenes.

Table 4: FTIR peaks for EVA extracted from the cells of module type I

Peaks		Unexposed		Module type I		
					Edges	Centers

	Functional groups	Uncured	Cured	Non-cell	A8	A9	B8	B9	B10	C8	C9	A8	A9	B8	B9	B10	C8	C9
719	**CH_2 vibration**	X	X	X	X	X	X	X	X	X	X	X	X	X	X	X	X	X
958	**CH_2-CH=CH_2**					X	X				X		X	X	X		X	X
962	**Alkenes**			X	X			X	X	X		X				X		
1018	**(COC) Ester**	X	X	X	X	X	X	X	X	X	X	X	X	X	X	X	X	X
1237	**(C-O) Ester**	X	X	X	X	X	X	X	X	X	X	X	X	X	X	X	X	X
1371	**CH_2 bending**	X	X	X	X	X	X	X	X	X	X	X	X	X	X	X	X	X
1435	**C-H bending**											X	X	X	X	X	X	X
1461	**$(CH_2)_{as}$ bending**	X	X	X	X	X	X	X	X	X	X	X	X	X	X	X	X	X
1576	**(C=C)**				X	X	X	X	X	X	X	X	X	X	X	X	X	X
1651	**Aromatic C=CH**						X	X							X	X		
1736	**(C=O) Ester**	X	X	X	X	X	X	X	X	X	X	X	X	X	X	X	X	X
2851	**$(CH_2)_s$ stretching**	X	X	X	X	X	X	X	X	X	X	X	X	X	X	X	X	X
2918	**$(CH_2)_{as}$ stretching**	X	X	X	X	X	X	X	X	X	X	X	X	X	X	X	X	X

Table 5: FTIR peaks for EVA extracted from the cells of module type II

Peaks		Unexposed		Module type II												
					Edges						Centers					
		Uncured	cured	Non-cell	A2	A7	B3	B5	B6	C8	A2	A7	B3	B5	B6	C8
719	CH_2 vibration	X	X	X	X	X	X	X	X	X	X	X	X	X	X	X

958	CH_2-CH=CH$_2$				X	X	X	X	X		X	X	X	X	X	X
962	Alkenes			X						X						
1018	(COC) Ester	X	X	X	X	X	X	X	X	X	X	X	X	X	X	X
1237	(C-O) Ester	X	X	X	X	X	X	X	X	X	X	X	X	X	X	X
1371	CH_2 bending	X	X	X	X	X	X	X	X	X	X	X	X	X	X	X
1461	$(CH_2)_{as}$ bending	X	X	X	X	X	X	X	X	X	X	X	X	X	X	X
1465	**C-H bending**						X		X		X	X	X	X		
1562	(C=C)			X	X	X	X	X	X	X	X	X	X	X	X	X
1736	(C=O) Ester	X	X	X	X	X	X	X	X	X	X	X	X	X	X	X
2851	$(CH_2)_s$ stretching	X	X	X	X	X	X	X	X	X	X	X	X	X	X	X
2918	(CH_2)as stretching	X	X	X	X	X	X	X	X	X	X	X	X	X	X	X

Table 6: FTIR peaks for EVA extracted from the cells of module type III

Peaks	**Functional groups**	**Unexposed**		**Module type III**								
					Edges				**Centers**			
		uncured	**cured**	**Non-cell**	**I11**	**I12**	**J11**	**J12**	**I11**	**I12**	**J11**	**J12**
719	CH_2 vibration	X	X	X	X	X	X	X	X	X	X	X
958	CH_2-CH=CH_2				X	X	X	X	X	X	X	X
962	Alkenes			X								
1018	(COC) Ester	X	X	X	X	X	X	X	X	X	X	X
1237	(C-O) Ester	X	X	X	X	X	X	X	X	X	X	X
1371	CH_2 bending	X	X	X	X	X	X	X	X	X	X	X
1461	$(CH_2)_{as}$ bending	X	X	X	X	X	X	X	X	X	X	X
1562	(C=C)			X		X	X	X		X	X	X
1736	(C=O) Ester	X	X	X	X	X	X	X	X	X	X	X
2851	$(CH_2)_s$ stretching	X	X	X	X	X	X	X	X	X	X	X

2918	(CH_2)as stretching	X	X									
2922	(CH_2)as stretching			X	X	X	X	X	X	X	X	X

4.9 Correlation between different characterization methods

Correlations were established to compare the effects of EVA degradation on its physical and chemical properties as well as on the performance of the glass/backsheet and glass/glass modules. Average values of the cell edges and the cell centers were considered to establish a relationship among the properties.

Figure 45 shows the relationship established between the degree of crosslinking, degree of crystallinity, vinyl acetate content (increase in degradation with the increase in VA content (%)) and yellowness index of EVA encapsulant (color change from transparent to dark brown with the increase in YI) in module type I due to its degradation. According to Figure 45 (a), for module type I, there is an increase in the degree of crosslinking and a decrease in the degree of crystallinity with the increase in vinyl acetate content. Similarly, according to Figure 45 (b), there is an increase in the degree of crosslinking and a decrease in the degree of crystallinity with the increase in the yellowness index. A similar observation is seen for module type II and type III in Figure 46 and Figure 47, respectively. Therefore, it can be concluded that VA content is directly related to the yellowness index of EVA i.e. higher the browning, higher is the VA content in the EVA encapsulant.

Another observation taken from Figure 45, Figure *46*, and Figure *47* is that an increase in the degree of crosslinking tends to cause a decrease in the degree of crystallinity. This is clearly because of crosslinking that is caused by UV rays and temperature interferes the

molecular packing of atoms in polyethylene molecule of EVA. Besides, the vinyl acetate group too interferes with the stereoregularity of polyethylene molecules and thereby restricts/reduces the degree of crystallinity.

Modules type I and II follow almost the same trend for EVA samples. The reason for the slight change in the trend due to the non-cell and cell edge regions in module type II could be because of the occurrence of photobleaching with an unknown rate w.r.t. the discoloration which could have caused uncertainties. Despite the uncertainties, EVA from the cell centers of modules type I and II indicate the highest degradation. However, in module type III, the trend for EVA samples for the module is reversed from that for the modules type I and II. In module type III, the non-cell region shows the highest degradation caused followed by cell edges and then the cell centers. This clarifies that photobleaching has not occurred in glass/glass module (type III) since it is hermetically sealed causing acetic acid to be entrapped inside with no escape route due to no spacing between the layers and absence of backsheet. This caused the escape path (non-cell region followed by the cell edges) to undergo higher degradation than the cell centers.

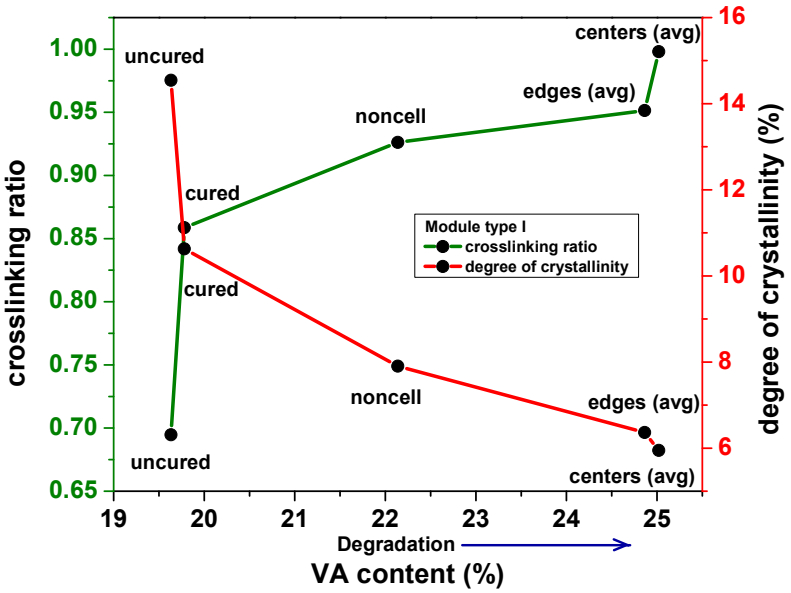
crosslinking ratio
degree of crystallinity (%)
VA content (%)
Degradation
Module type I
crosslinking ratio
degree of crystallinity
uncured
cured
noncell
edges (avg)
centers (avg)
cured
uncured
noncell
edges (avg)
centers (avg)
1.00
0.95
0.90
0.85
0.80
0.75
0.70
0.65
16
14
12
10
8
6
19
20
21
22
23
24
25

(a)

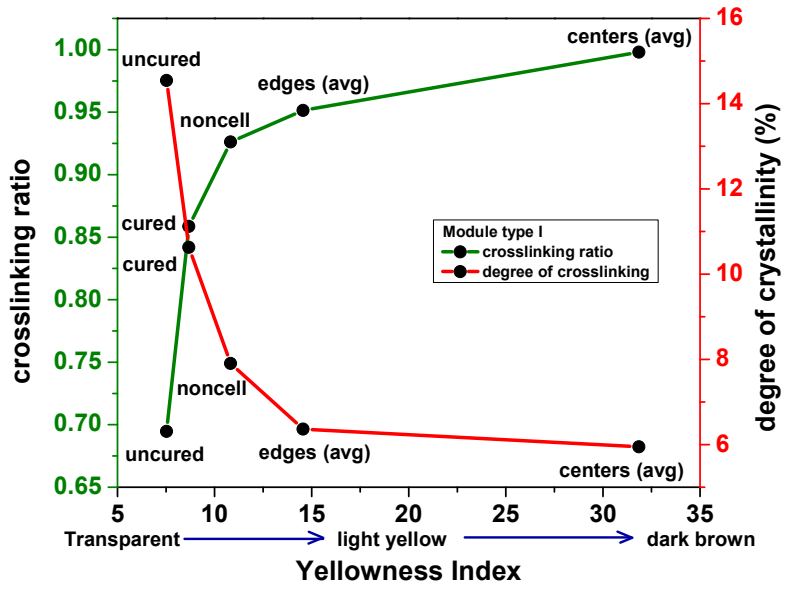
crosslinking ratio
degree of crystallinity (%)
Yellowness Index
Transparent
light yellow
dark brown
Module type I
crosslinking ratio
degree of crosslinking
uncured
edges (avg)
noncell
cured
cured
noncell
uncured
edges (avg)
centers (avg)
centers (avg)
1.00
0.95
0.90
0.85
0.80
0.75
0.70
0.65
16
14
12
10
8
6
5
10
15
20
25
30
35

(b)

Figure 45: Correlations between (a) crosslinking ratio, VAc, and degree of crystallinity, and (b) crosslinking ratio, YI and degree of crystallinity for module type I

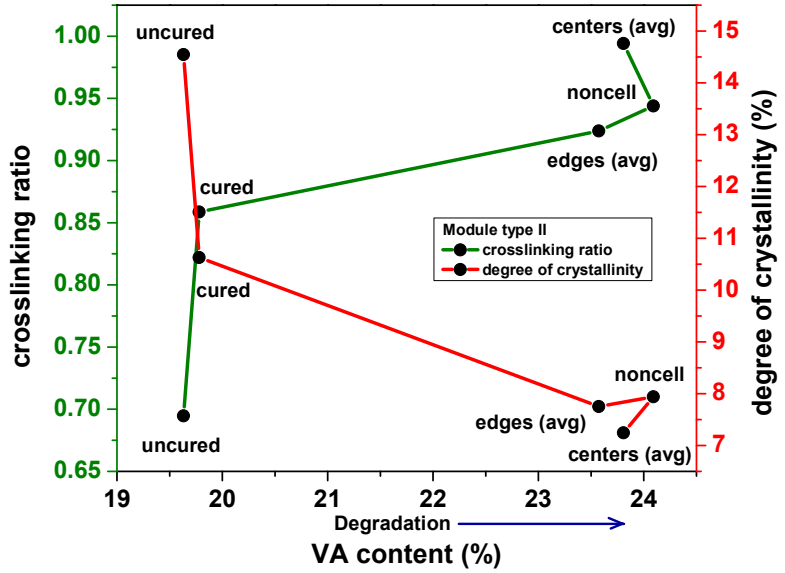

(a)

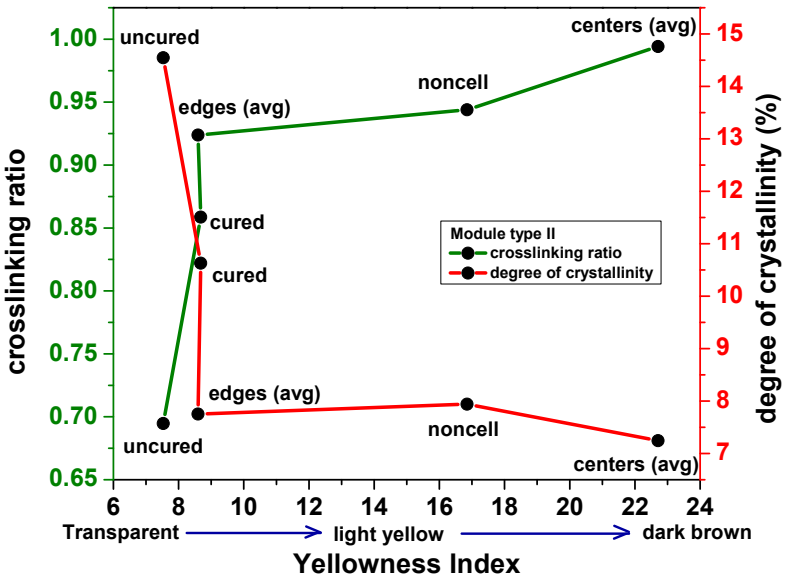

(b)

Figure 46: Correlations between (a) crosslinking ratio, VAc, and degree of crystallinity, and (b) crosslinking ratio, YI and degree of crystallinity for module type II

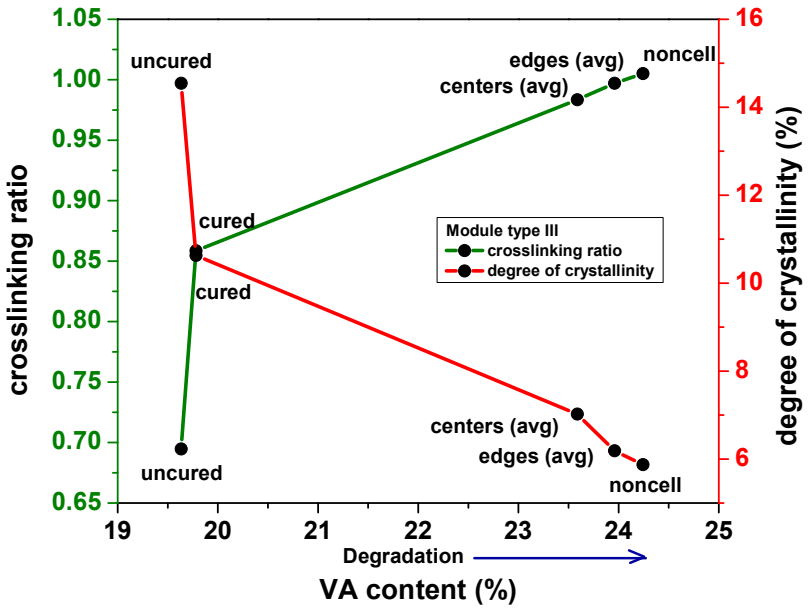

(a)

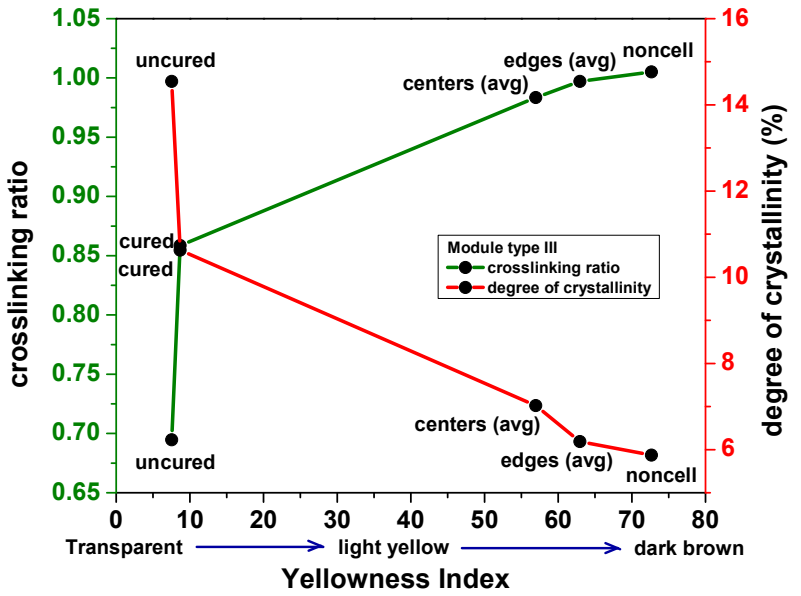

(b)

Figure 47: Correlations between (a) crosslinking ratio, VAc, and degree of crystallinity, and (b) crosslinking ratio, YI and degree of crystallinity for module type III

Figure 48 relates the change in performance parameters to the changes in physical and chemical properties of the EVA encapsulant caused due to its degradation. Yellowness index is related to the I_{sc} and P_{max} degradation rates (%/year). I_{sc} degradation rate for the modules is linearly proportional to the yellowness index. Hence, yellowness index along with I_{SC} degradation rate for the glass/glass module is higher than that of glass/backsheet modules (type I and type II). For glass/backsheet modules, even though type II has higher field exposure than type I, it seems to be having lower YI as well as lower performance losses compared to type I. One reason could be because the module type II had several cracked cells in the modules which could have provided a pathway for oxygen to cause photobleaching which could have lowered the degradation rates. Therefore, I_{SC} is drastically affected by encapsulant browning because degradation alters and worsens the optical properties of the encapsulant. Since I_{sc} is one of the factors contributing to P_{max}, P_{max} also decreases with an increase in browning. Also, another observation is that the YI order and I_{sc} degradation rate (%/year) order is exactly the same indicating that the I_{sc} loss is predominantly coming from EVA browning.

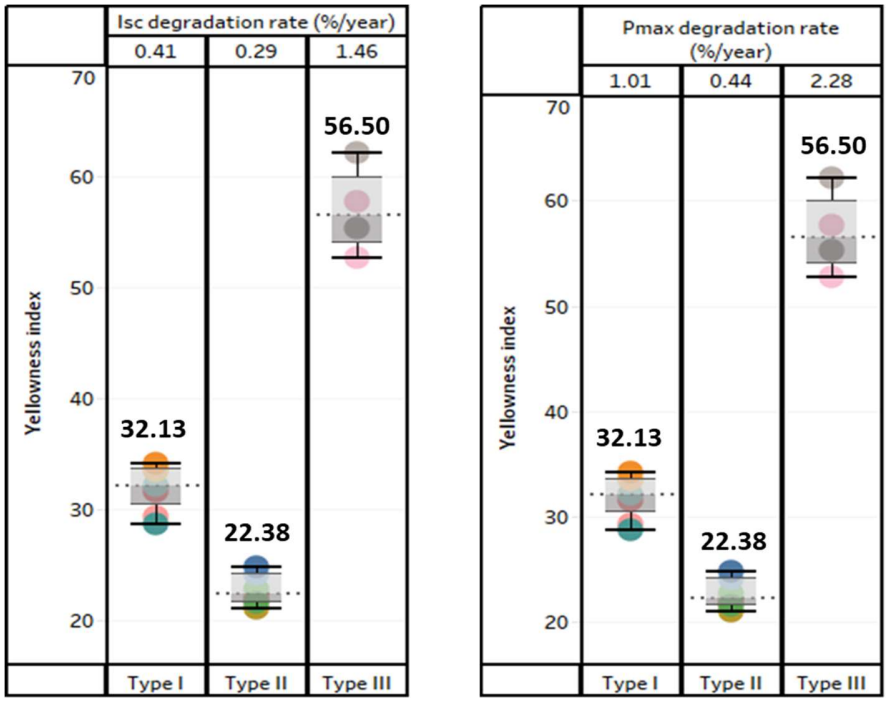

Figure 48: Correlation of YI with (a) I_{sc}, and (b) P_{max} for modules type I, type II, and type II

5. CONCLUSION

The EVA browning in two different module constructions – glass/backsheet (modules type I and II) and glass/glass (type III) modules after a prolonged field exposure is investigated using different characterization techniques.

The following conclusions were drawn from the characterization techniques performed on EVA samples:

- When EVA undergoes degradation due to high UV radiation and elevated temperature, UV light attacks the terminal CH_3 group of vinyl acetate group transforming it into CH_2 groups which leads to an increase in the degree of crosslinking. This can be concluded from the results obtained from Raman spectroscopy.
- Crosslinking interferes the orderly packing of polyethylene molecules and reduces the molecular weight of EVA, hence causes a decrease in crystallinity of the encapsulant which is confirmed from the results obtained from DSC.
- The decrease in crystallinity consequently leads to an increase in the amorphous content in the polymer. Here, vinyl acetate content which is the amorphous part of the EVA copolymer increases which can be verified from the results obtained from TGA. Higher the VA content, higher is the production of acetic acid which further catalyzes the degradation reaction.

- Apart from the increase in crosslinking, deacetylation reaction occurs due to UV rays and temperature to produce acetic acid and long chain polyenes $\{C=C\}_n$. Presence of polyenes can be detected in FTIR results.
- Polyenic chromophores cause browning of the EVA encapsulant. Longer chain polyenes cause higher discoloration of EVA. Photobleaching causes oxidation of long-chain polyenes converting them into shorter chain polyenes due to which the intensity of polyenes decreases, and the brown color of EVA goes back to being faint yellow or white which has been verified from colorimetric measurements.
- Higher discoloration of EVA causes higher current losses which were verified by the I-V measurements. It appears that majority of the loss in power is due to current loss (rather than voltage or fill factor loss) which in turn is due to EVA browning issue.

On comparing the glass/backsheet (modules type I and II) and glass/glass (module type III) modules, it is evident that about 45% of power loss is coming from I_{sc} loss in glass/backsheet modules whereas about 65% of power loss is coming from I_{sc} loss in glass/glass and encapsulant browning has a major role to play in it because degradation rates of the performance parameters per year are directly proportional to the yellowness index of the encapsulant. The yellowness indices for EVA extracted from glass/glass module are much higher than that from glass/backsheet modules. This concludes that higher EVA encapsulant discoloration is caused in glass/glass module than in glass/backsheet modules because unlike glass/backsheet modules, glass/glass module does not have a breathable backsheet which can allow the volatile acetic acid to diffuse out.

Instead, acetic acid and other volatile compounds are entrapped in the glass/glass module which causes the autocatalytic reaction, accelerating the EVA encapsulant browning. The absence of a cell in the inter-cell regions doubles the thickness of the EVA in the non-cell region causes higher penetration of UV rays into the second layer of EVA leading to higher crosslinking and higher production of acetic acid and polyenes. With no breathable backsheet as an escape route for the produced acetic acid, the browning intensifies in the non-cell region of glass/glass module with double layer EVA unlike in glass/backsheet modules where the volatile compounds present in the non-cell double layer EVA region and EVA from cell edges diffuse out through the shortest path available through the backsheet and absence of acetic acid in those regions does not accelerate the degradation process. From the observations, it is evident that EVA might be a good choice of an encapsulant for glass/backsheet modules, but it does not seem to be quite the apt choice for glass/glass modules because it almost doubles the current losses when compared to that of the glass/backsheet modules. This conclusion based on the limited number of samples needs to be further validated using a statistically significant number of field-aged and/or accelerated tested glass/glass modules.

Some of the suggestions for future scope of work:

- It would be helpful to study degradation mechanisms of other encapsulants such as POE, ionomer, etc. that are commercially used in the PV market for modules of different constructions.

- Since the encapsulants have various additives to achieve maximum efficiency or reliability/durability, it is important to study the role of additives in encapsulant degradation.
- To study the effects of encapsulant degradation on other layers of the module i.e. encapsulant delamination and corrosion on cell metallization caused by acetic acid.

REFERENCES

[1] A. Perea *et al.*, "U.S. Solar Market Insight-Executive Summary," GTM Research, U.S., 2017.

[2] A. W. Czanderna and G. J. Jorgensen, "Service Lifetime Prediction for Encapsulated Photovoltaic cells/Minimodules," *AIP Conf. Proc.*, pp. 295–312, 1997.

[3] R. Polanský, M. Pinkerová, M. Bartůňková, and P. Prosr, "Mechanical behavior and thermal stability of eva encapsulant material used in photovoltaic modules," *J. Electr. Eng.*, vol. 64, no. 6, pp. 361–365, 2013.

[4] M. C. C. de Oliveira, A. S. A. Diniz Cardoso, M. M. Viana, and V. de F. C. Lins, "The causes and effects of degradation of encapsulant ethylene vinyl acetate copolymer (EVA) in crystalline silicon photovoltaic modules: A review," *Renew. Sustain. Energy Rev.*, vol. 81, no. June, pp. 2299–2317, 2018.

[5] "Ethylene-vinyl acetate," 2015. [Online]. Available: https://en.wikipedia.org/wiki/Ethylene-vinyl_acetate. [Accessed: 27-Oct-2018].

[6] T. R. B. and R. G. Dan Wu*, Jiang Zhu and Centre, "Degradation of interfacial adhesion strength within photovoltaic mini-modules during damp-heat exposure," *Prog. Photovoltaics Res. Appl.*, vol. 9, no. 11, pp. 261–270, 2014.

[7] F. J. Pern, "Factors that affect the EVA encapsulant discoloration rate upon accelerated exposure," *Sol. Energy Mater. Sol. Cells*, vol. 41–42, pp. 587–615, 1996.

[8] A. W. Czanderna and F. J. Pern, "Encapsulation of PV modules using ethylene vinyl acetate copolymer as a pottant: A critical review," *Sol. Energy Mater. Sol. Cells*, vol. 43, no. 2, pp. 101–181, 1996.

[9] F. J. Pern and A. W. Czanderna, "Characterization of ethylene vinyl acetate (EVA) encapsulant: Effects of thermal processing and weathering degradation on its discoloration," *Sol. Energy Mater. Sol. Cells*, vol. 25, no. 1–2, pp. 3–23, 1992.

[10] A. W. Czanderna and F. J. Pern, "Encapsulation of PV modules using ethylene vinyl acetate copolymer as a pottant: A critical review," *Sol. Energy Mater. Sol. CellsJ. Pern / Sol. Energy Mater. Sol. Cells*, vol. 43, no. 43, pp. 101–181, 1996.

[11] Mike Rycroft (EE publishers), "Solar PV module faults and failings," Sep-2016.

[12] E. Kaplani, "Degradation Effects in sc-Si PV Modules Subjected to Natural and Induced Ageing after Several Years of Field Operation," *J. Eng. Sci. Technol. Rev.*, p. 23, 2012.

[13] K. Agroui and G. Collins, “Thermal relaxations and transitions in EVA encapsulant material during photovoltaic module encapsulation process,” *Mater. Process. energy Commun. Curr. Res. Technol. Dev.*, pp. 150–157, 2013.

[14] C. Peike, T. Kaltenbach, K. A. Weiß, and M. Koehl, “Non-destructive degradation analysis of encapsulants in PV modules by Raman Spectroscopy,” *Sol. Energy Mater. Sol. Cells*, vol. 95, no. 7, pp. 1686–1693, 2011.

[15] C. Peike, W. Phondongnok, T. Kaltenbach, and M. Koehl, “Non-destructive determination of the cross-linking degree of EVA by Raman Spectroscopy,” vol. 1, no. 1, pp. 14–21, 2014.

[16] E. Planes, B. Yrieix, C. Bas, and L. Flandin, “Chemical degradation of the encapsulation system in flexible PV panel as revealed by infrared and Raman microscopies,” *Sol. Energy Mater. Sol. Cells*, vol. 122, pp. 15–23, 2014.

[17] F. J. Pern, “Ethylene-Vinyl Acetate (EVA) Encapsulant for Photovoltaic Modules : Degradation and Discoloration Mechanisms and Formulation Modifications for Improved Photostability,” *Macromol. Mater. Eng.*, vol. 252, pp. 195–216, 1997.

[18] K. Dolia, “Accelerated UV Testing and Characterization of PV Modules with UV-cut and UV-pass EVA Encapsulants,” MS Thesis, Arizona State University, 2018.

[19] S. J. C. X. M. Shi, J. Zhang*, J. Jin, “Non-isothermal crystallization and melting of ethylene-vinyl acetate copolymers with different vinyl acetate contents,” *eXPRESS Polym. Lett.*, vol. 2, no. 10, pp. 623–629, 2008.

[20] S. Bistac, P. Kunemann, and J. Schultz, “Crystalline modifications of ethylene-vinyl acetate copolymers induced by a tensile drawing: Effect of the molecular weight,” *Polymer (Guildf).*, vol. 39, no. 20, pp. 4875–4881, 1998.

[21] C. C. Ibeh, “Crystallinity and Crystallization in Polymers and Plastics,” in *Thermoplastic Materials: Properties, Manufacturing Methods, and Applications*, First., 2011, p. 640.

[22] M. Chicca, “Characterization and Analysis of Long-Term Field Aged Photovoltaic Modules and Encapsulant Materials,” MS Thesis, Arizona State University, 2015.

[23] C. Hirschl *et al.*, “Determining the degree of crosslinking of ethylene vinyl acetate photovoltaic module encapsulants - A comparative study,” *Sol. Energy Mater. Sol. Cells*, vol. 116, pp. 203–218, 2013.

[24] B. S. Chernev, C. Hirschl, and G. C. Eder, “Non-destructive determination of ethylene vinyl acetate cross-linking in photovoltaic (PV) modules by Raman

spectroscopy," *Appl. Spectrosc.*, vol. 67, no. 11, pp. 1296–1301, 2013.

[25] D. Wu, "Investigation of the reliability of the encapsulation system of photovoltaic modules," 2015.

[26] M. Kraft, M. De Biasio, C. Hirschl, and L. Neumaier, "In-line Raman Analysis of Ethylene Vinyl Acetate Curing for and in Industrial PV Module Manufacturing," no. August, 2015.

APPENDIX A

CHARACTERIZATION PLOTS FOR MODULE TYPE I

A.1. DSC plots

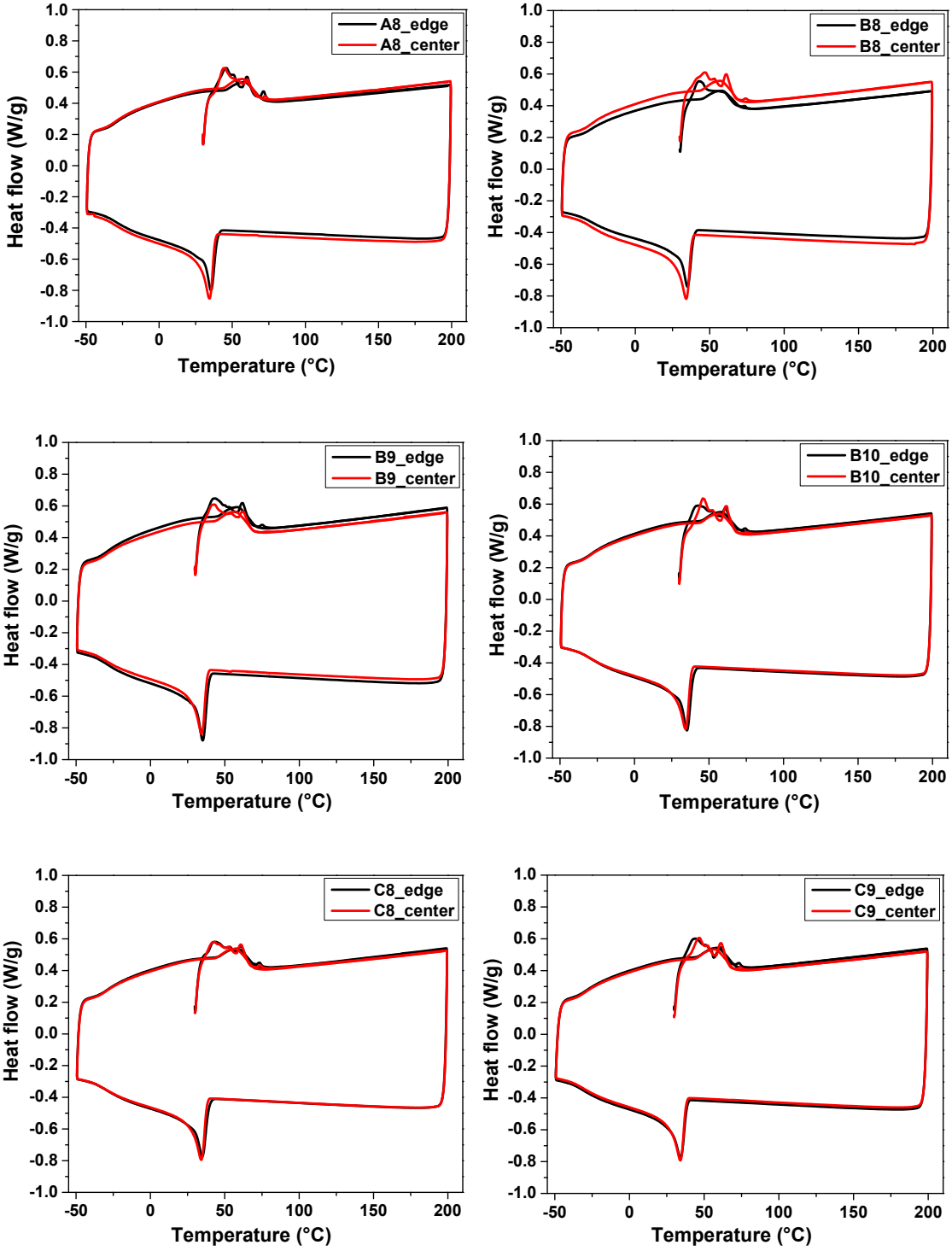
A8_edge
A8_center
B8_edge
B8_center
B9_edge
B9_center
B10_edge
B10_center
C8_edge
C8_center
C9_edge
C9_center
Heat flow (W/g)
Temperature (°C)

A.2. TGA plots

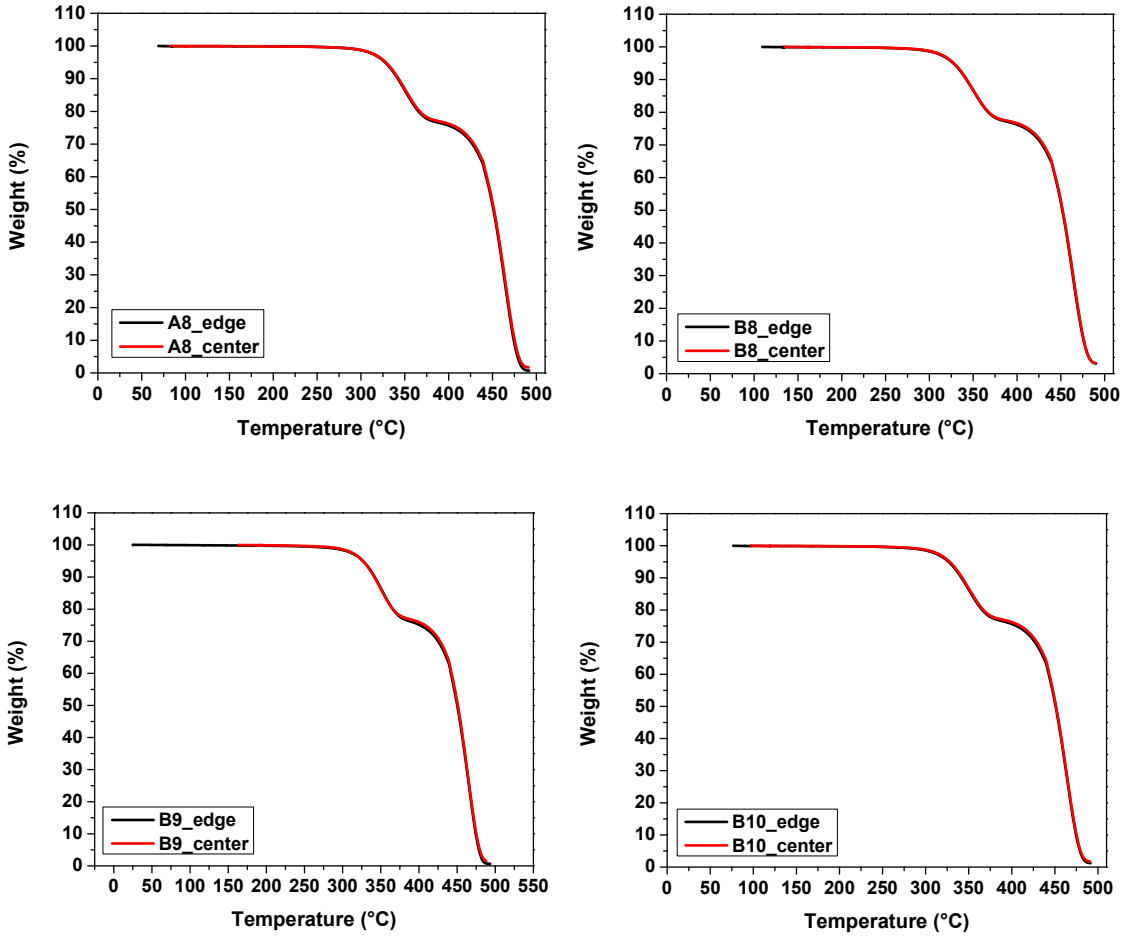
Weight (%)
Temperature (°C)
A8_edge
A8_center
B8_edge
B8_center
B9_edge
B9_center
B10_edge
B10_center

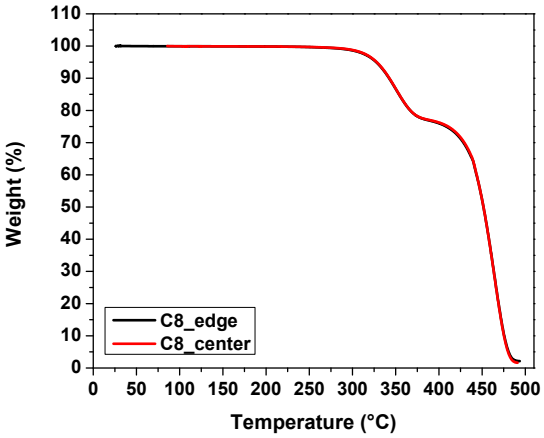

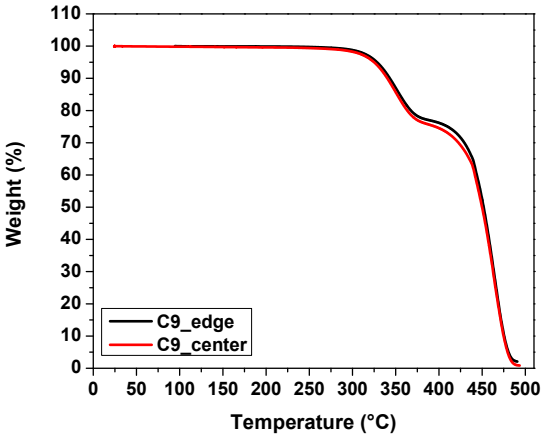

A.3. Raman plots

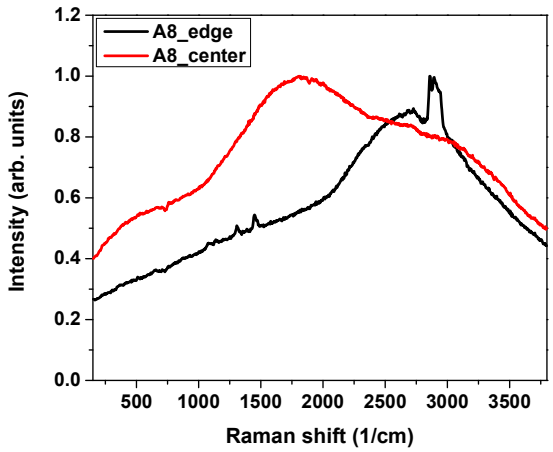

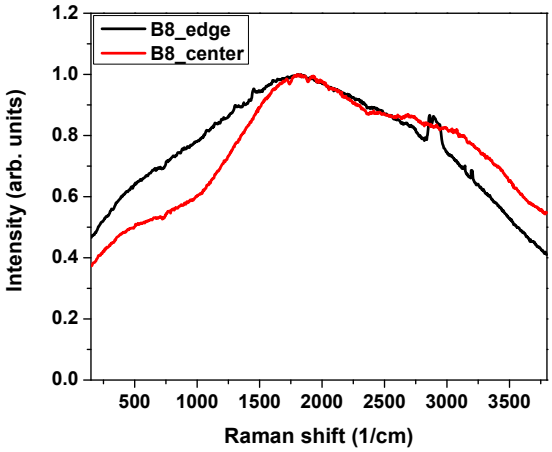

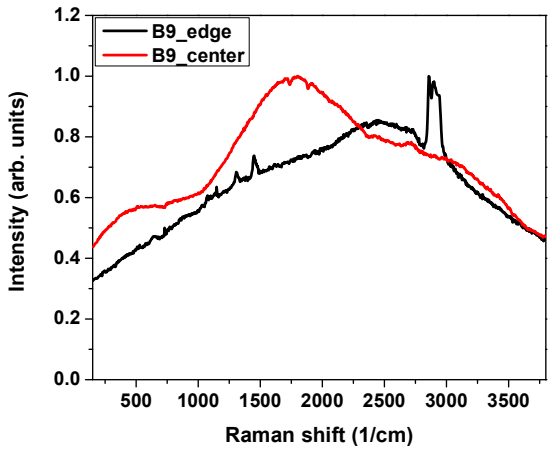

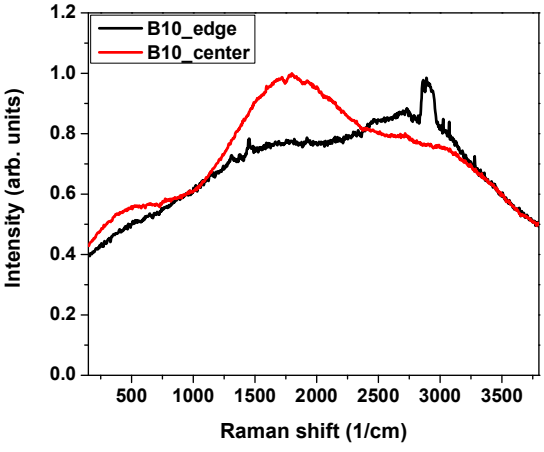

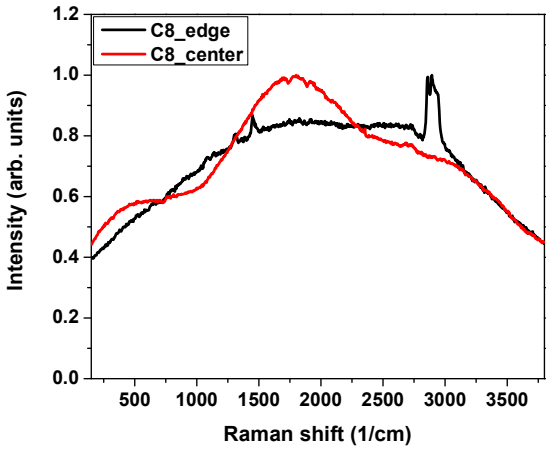

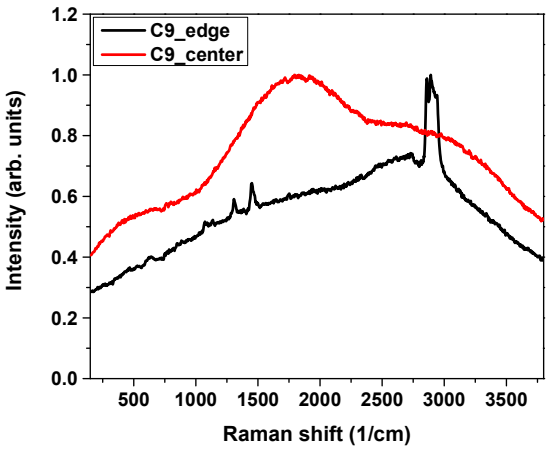

A.4. FTIR plots

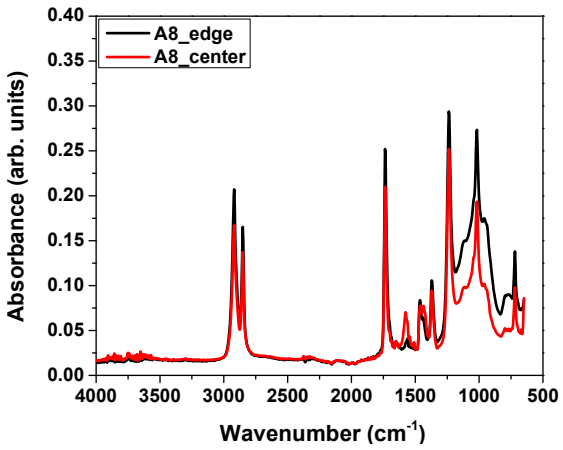

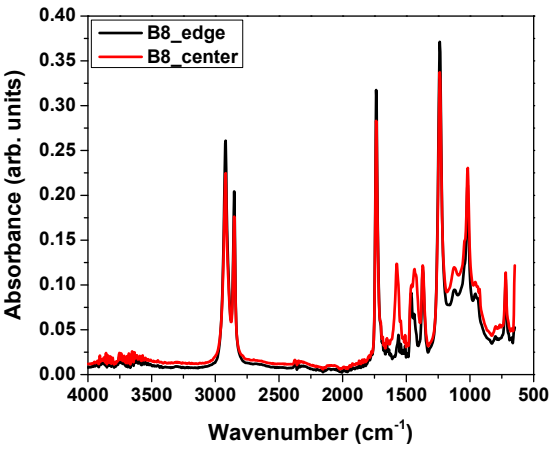

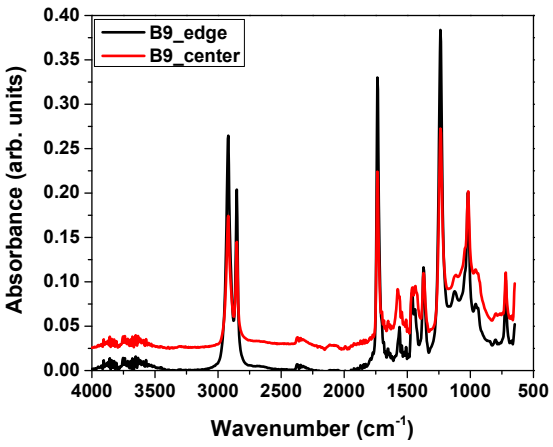

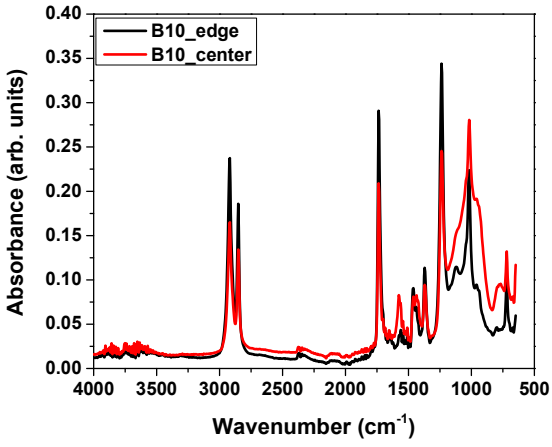

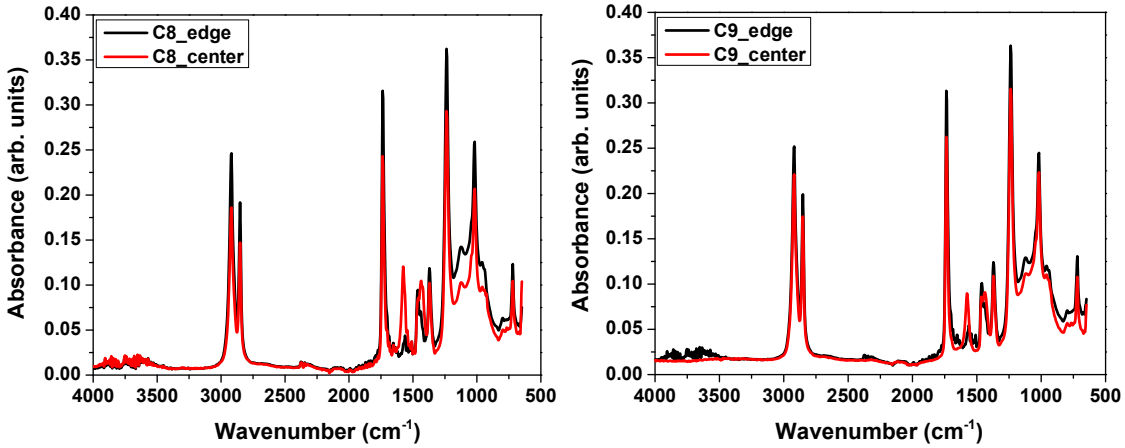
C8_edge
C8_center
Absorbance (arb. units)
Wavenumber (cm-1)
C9_edge
C9_center
Absorbance (arb. units)
Wavenumber (cm-1)

APPENDIX B

CHARACTERIZATION PLOTS FOR MODULE TYPE II

B.1. DSC plots

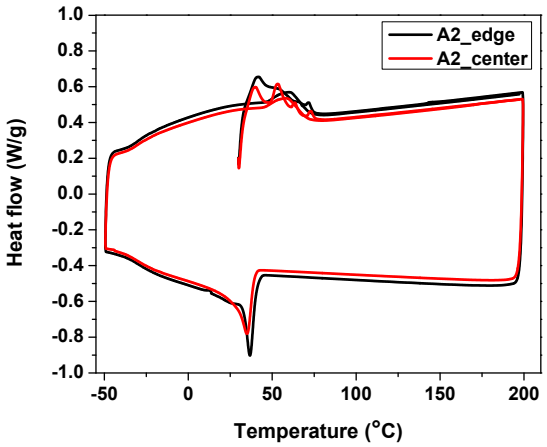
A2_edge
A2_center
Heat flow (W/g)
Temperature (°C)

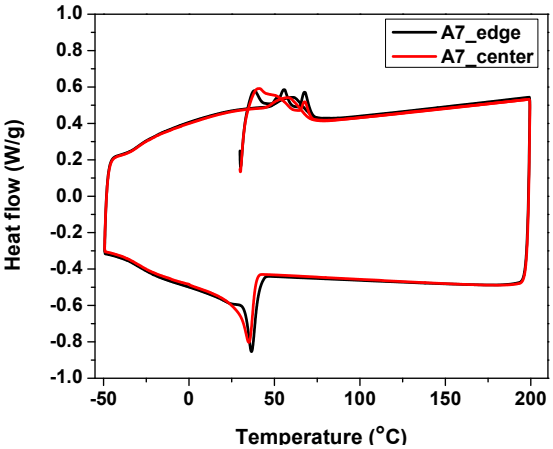
A7_edge
A7_center
Heat flow (W/g)
Temperature (°C)

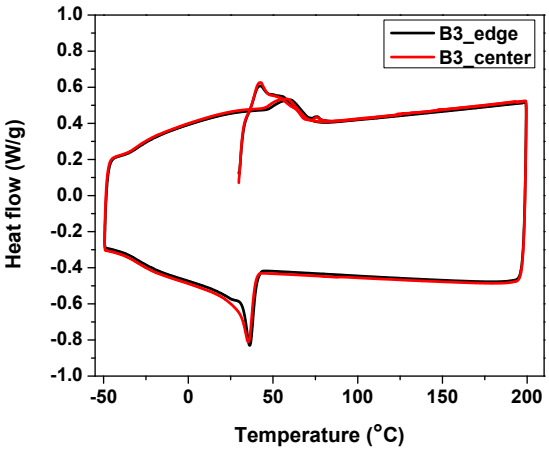
B3_edge
B3_center
Heat flow (W/g)
Temperature (°C)

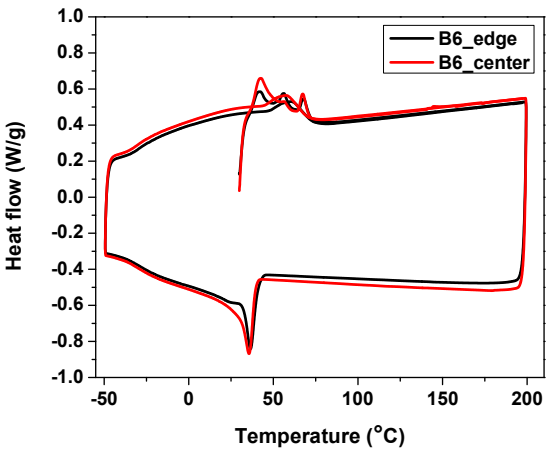
B6_edge
B6_center
Heat flow (W/g)
Temperature (°C)

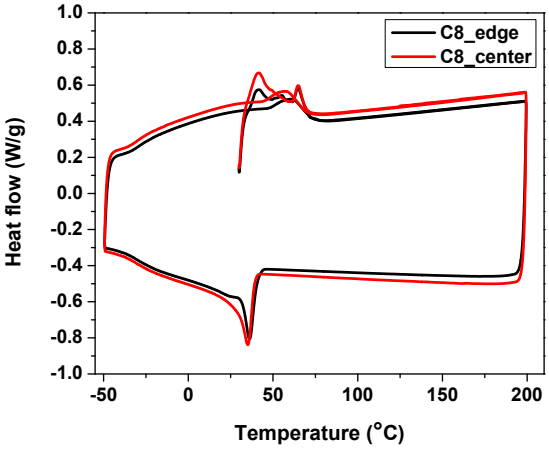
C8_edge
C8_center
Heat flow (W/g)
Temperature (°C)

B.2. TGA plots

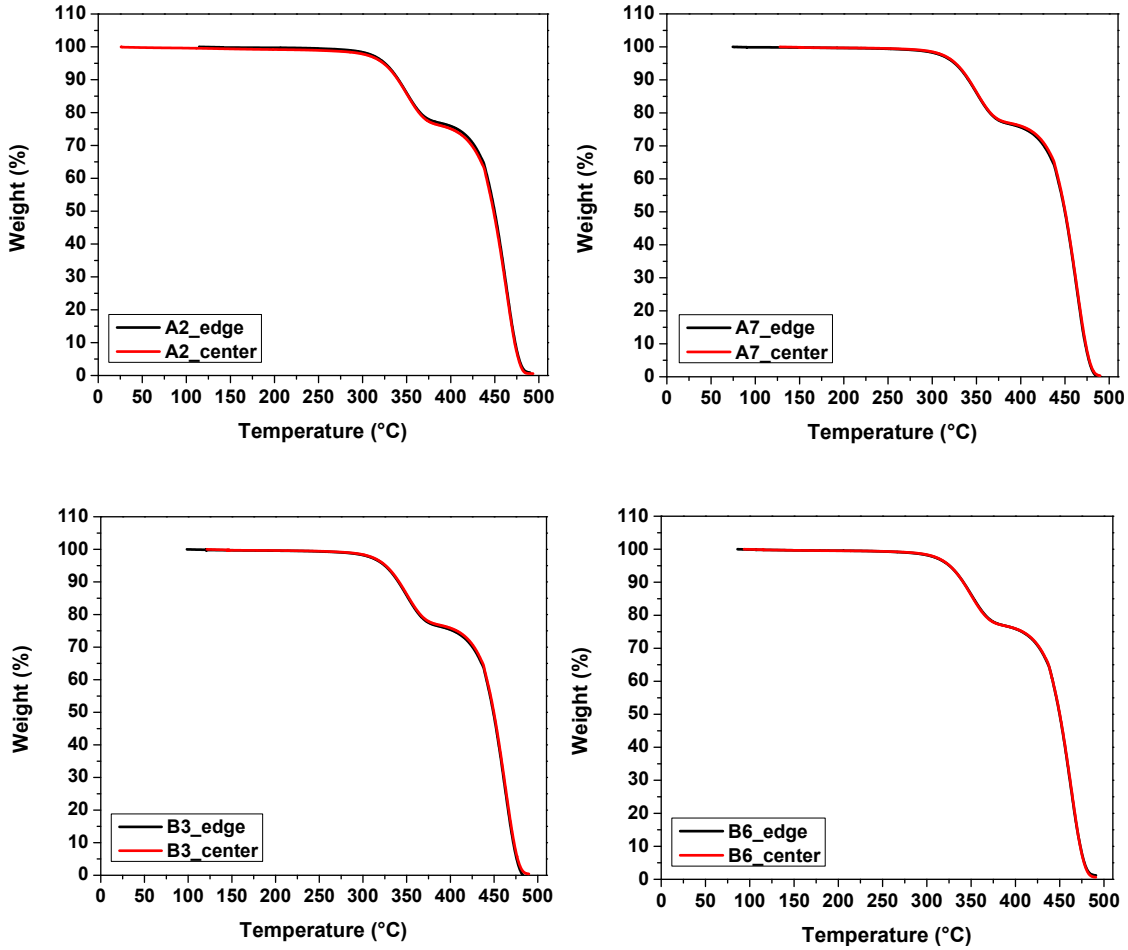
Weight (%)
Temperature (°C)
A2_edge
A2_center
A7_edge
A7_center
B3_edge
B3_center
B6_edge
B6_center

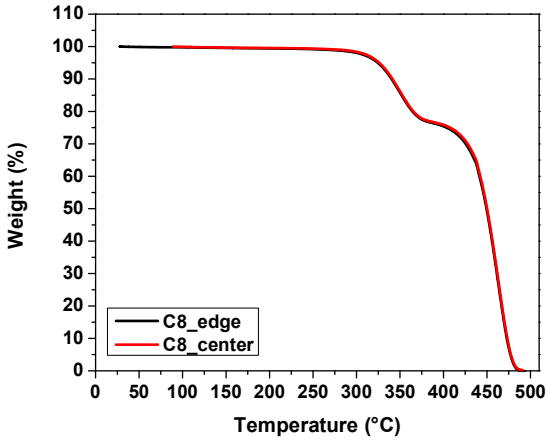

B.3. Raman plots

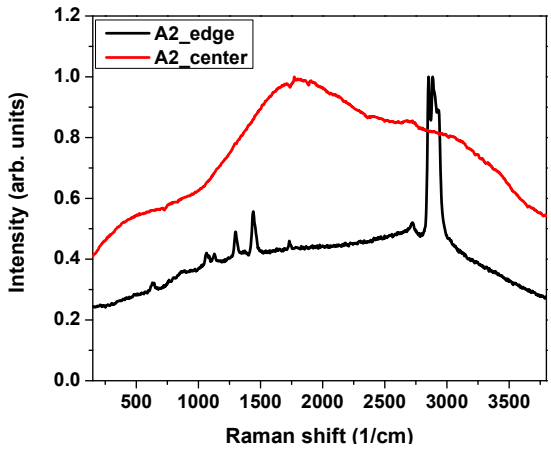

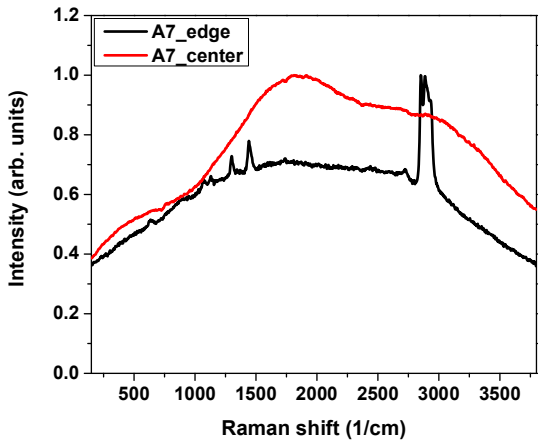

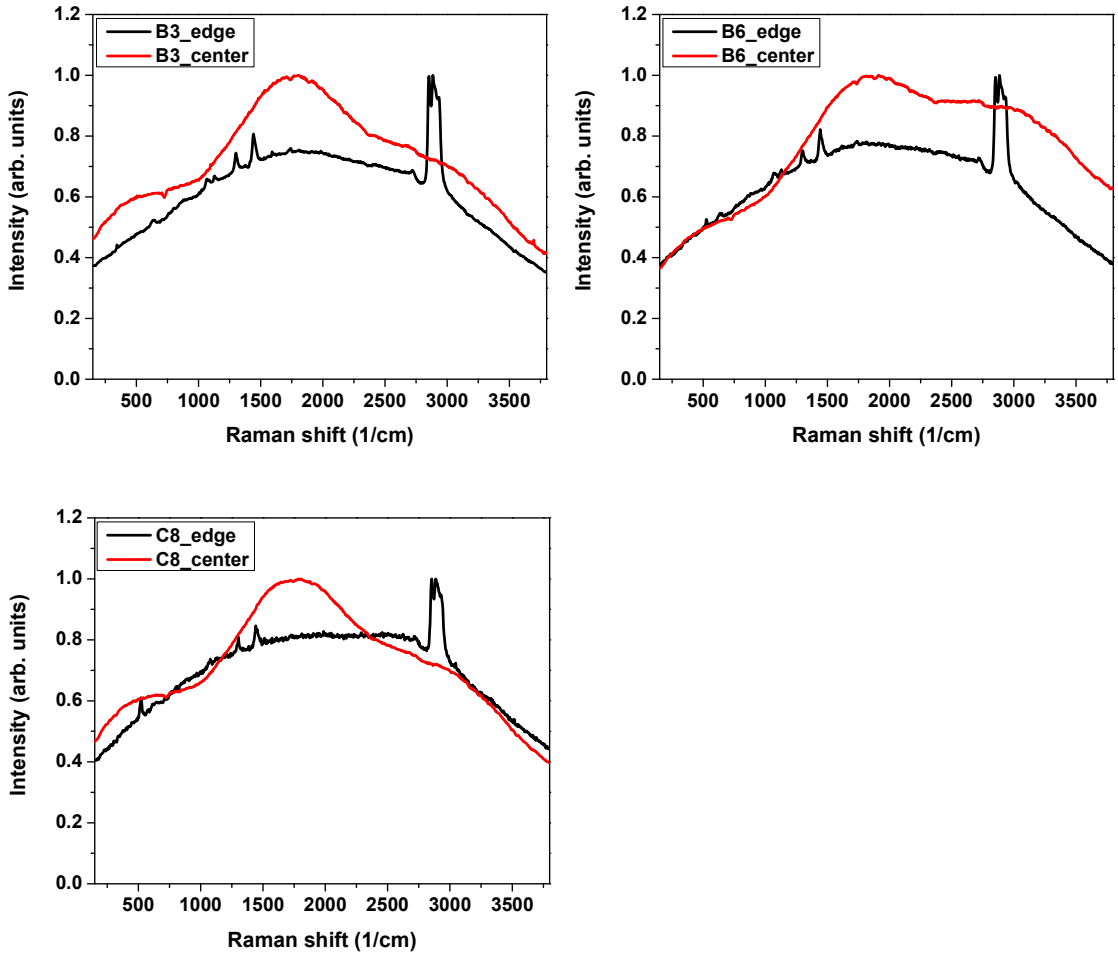

B.4. FTIR plots

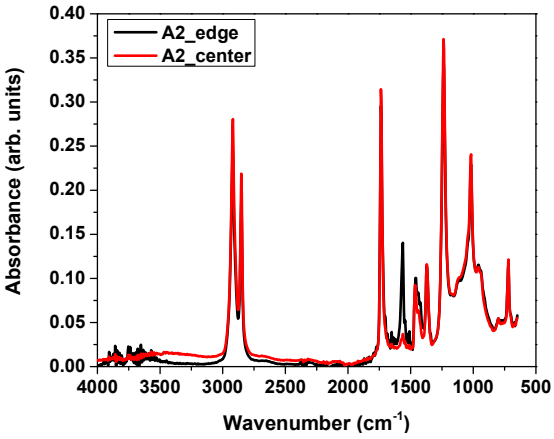
A2_edge
A2_center
Absorbance (arb. units)
Wavenumber (cm-1)

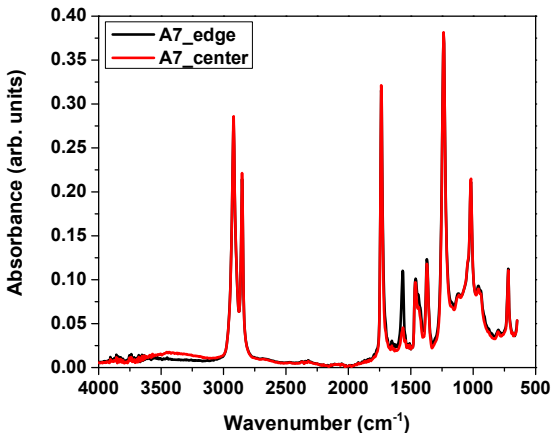
A7_edge
A7_center
Absorbance (arb. units)
Wavenumber (cm-1)

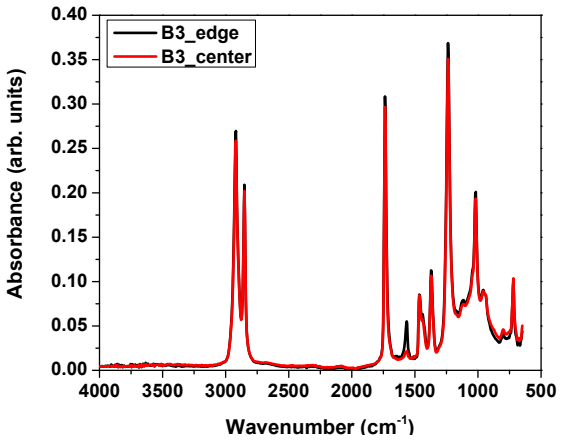
B3_edge
B3_center
Absorbance (arb. units)
Wavenumber (cm-1)

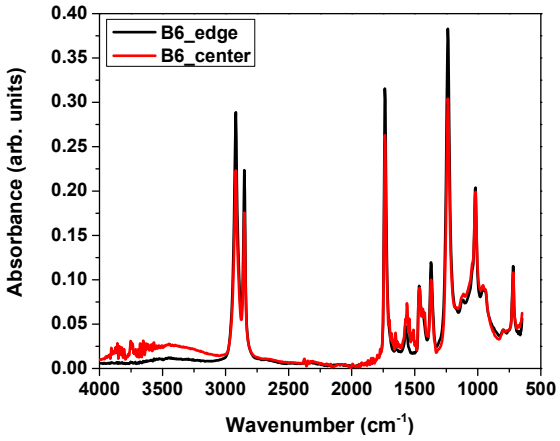
B6_edge
B6_center
Absorbance (arb. units)
Wavenumber (cm-1)

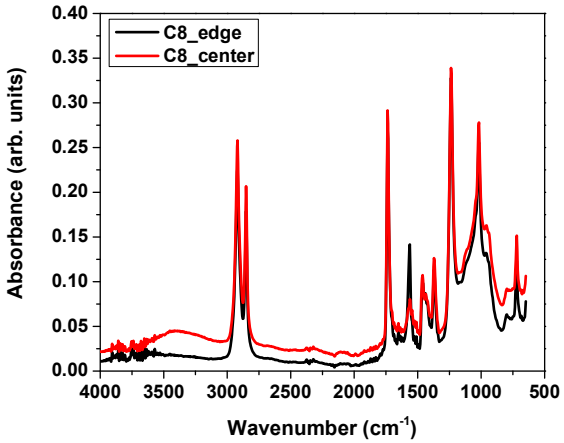
C8_edge
C8_center
Absorbance (arb. units)
Wavenumber (cm-1)

APPENDIX C

CHARACTERIZATION PLOTS FOR MODULE TYPE III

C.1. DSC plots

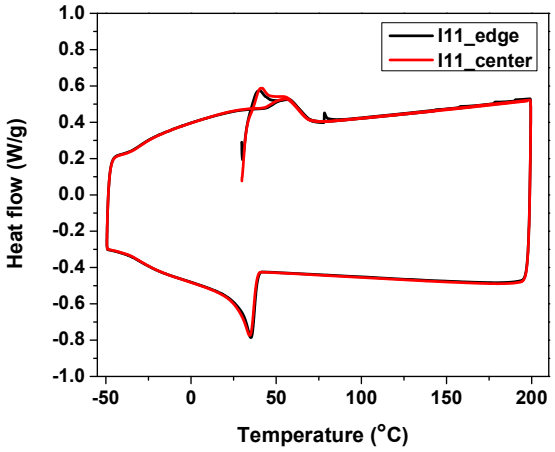

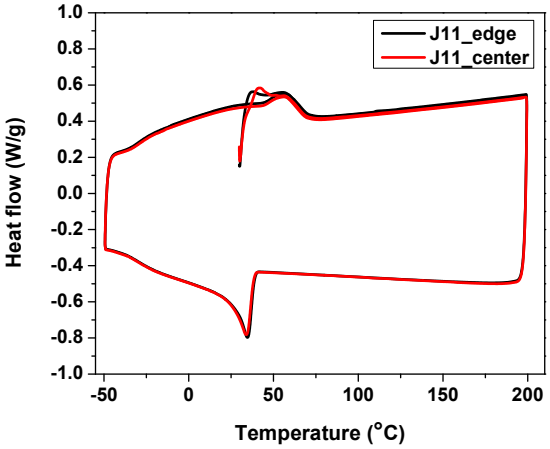

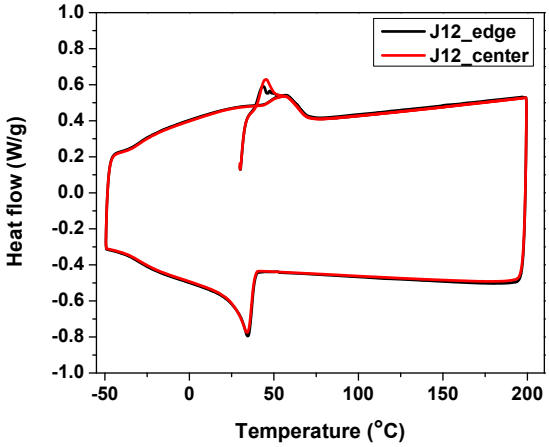

C.2. TGA plots

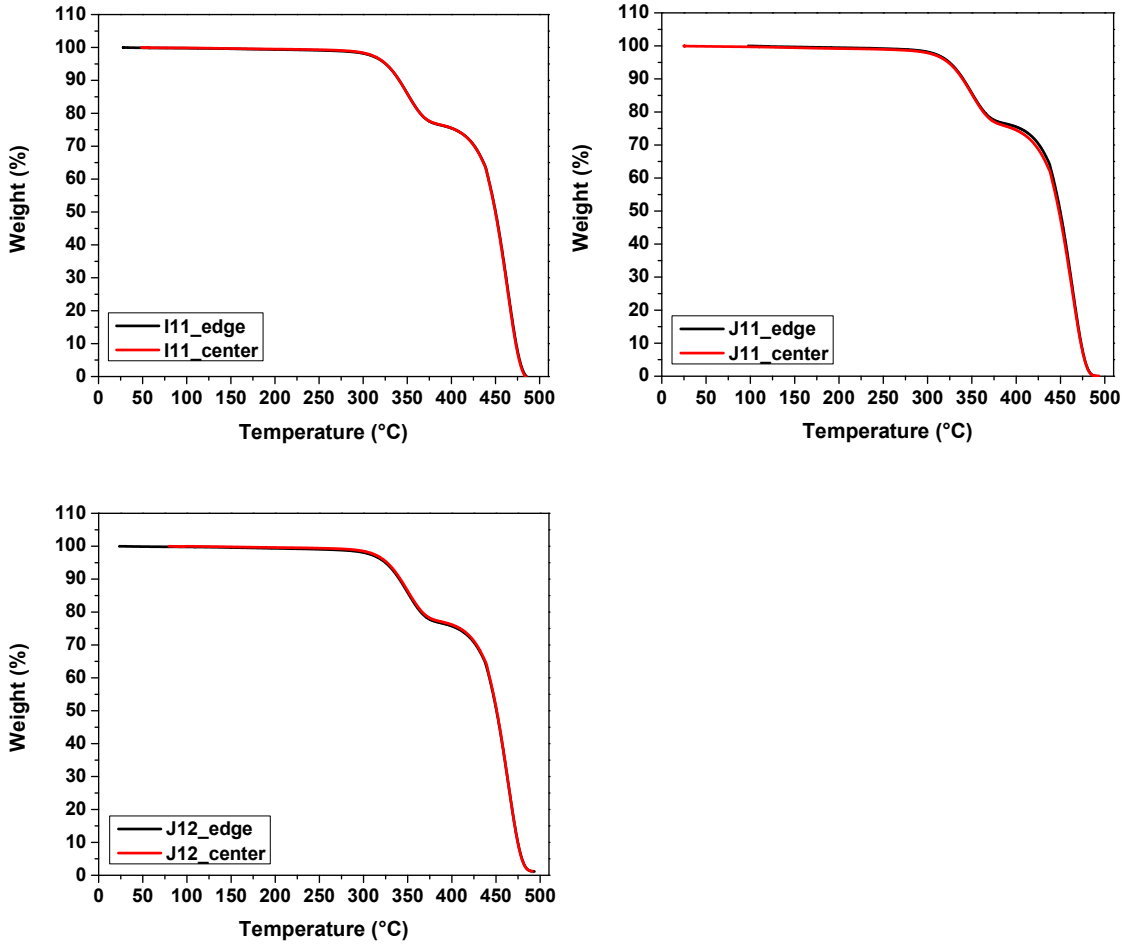

C.3. Raman plots

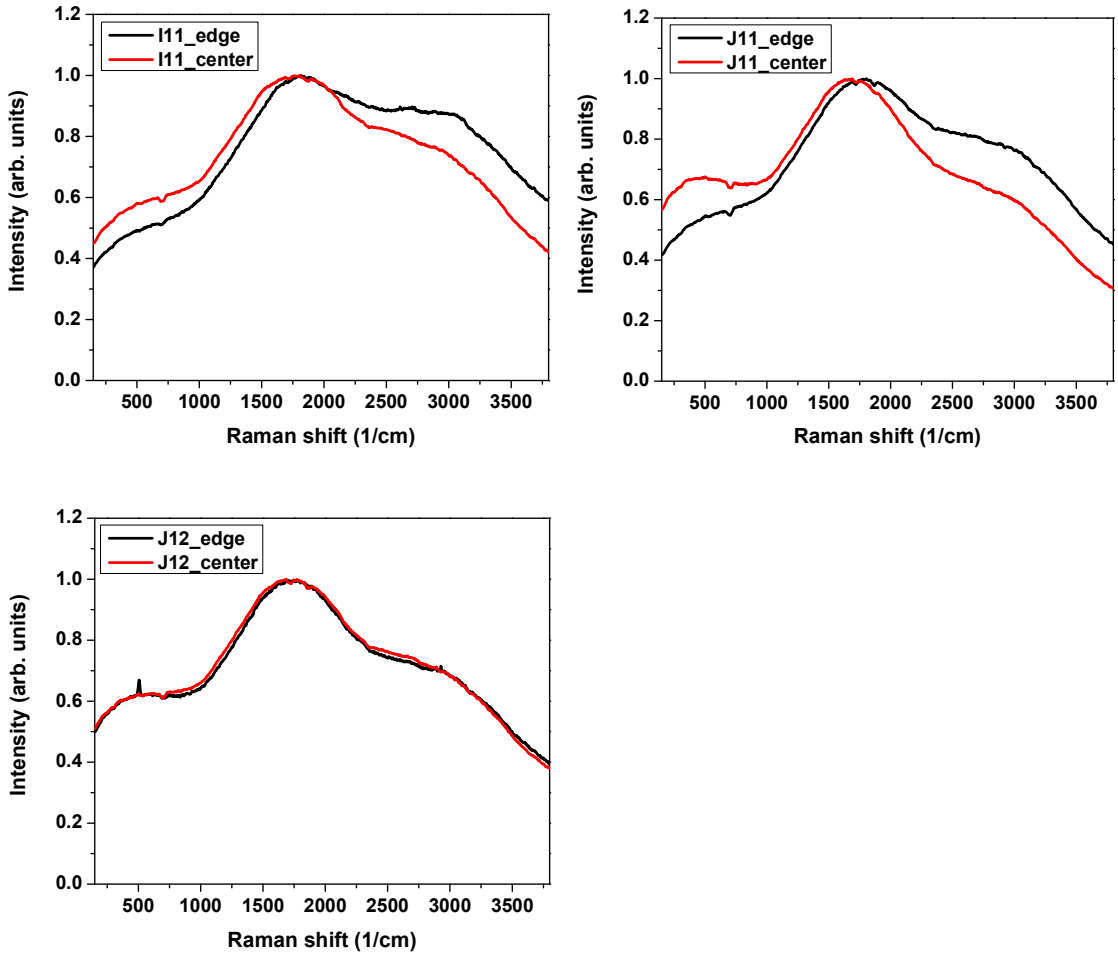

C.4. FTIR plots

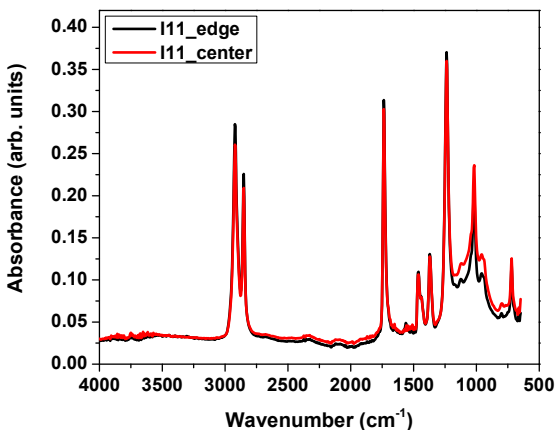
I11_edge
I11_center
Absorbance (arb. units)
Wavenumber (cm-1)

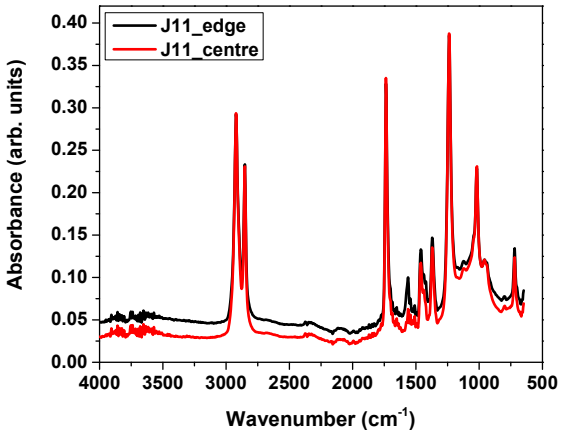
J11_edge
J11_centre
Absorbance (arb. units)
Wavenumber (cm-1)

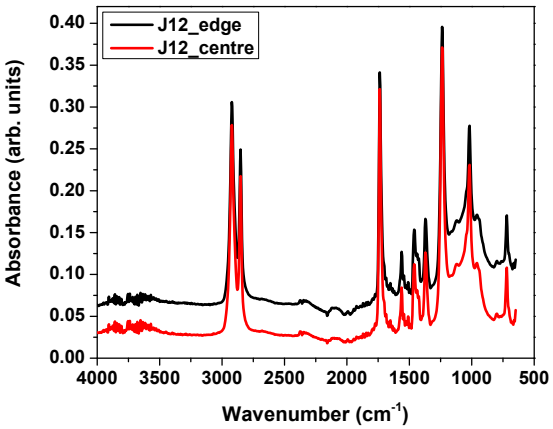
J12_edge
J12_centre
Absorbance (arb. units)
Wavenumber (cm-1)